DOI:10.14753/SE.2022.2739

SEMMELWEIS EGYETEM

DOKTORI ISKOLA

Ph.D. értekezések

2739.

BOZSÁNYI SZABOLCS

Bőrgyógyászat és venerológia

című program

Programvezető: Dr. Sárdy Miklós, egyetemi tanár

Témavezető: Dr. Wikonkál Norbert, egyetemi tanár

DOI:10.14753/SE.2022.2739

QUANTITATIVE MULTISPECTRAL IMAGING FOR THE DIAGNOSIS AND TUMOR DEPTH ASSESSMENT OF MALIGNANT MELANOMA

PhD thesis

Szabolcs Bozsányi, MD

KÁROLY RÁCZ DOCTORAL SCHOOL OF CLINICAL MEDICINE
Semmelweis University

Supervisor:	Prof. Norbert M. Wikonkál, MD, PhD, DSc
Official reviewers:	Ágota Szepesi, MD, PhD
	Tímea Balatoni, MD, PhD

Head of the Complex Examination Committee: Prof. Miklós Csala, MD, PhD, DSc

Members of the Complex Examination Committee: Barbara Molnár-Érsek, PhD, Eszter Baltás, MD, PhD

Budapest

2022

DOI:10.14753/SE.2022.2739

Table of Contents

List of Abbreviations

AF	Autofluorescence/autofluorescent
ALM	Acral lentiginous melanoma
DS	Dermoscope/dermatoscope
G	Green wavelength band
GP	General physician
HFUS	High-frequency ultrasound
LMM	Lentigo maligna melanoma
MM	Malignant melanoma
MSI	Multispectral imaging
NM	Nodular melanoma
NPD	Non-polarized dermatoscopy
IR	Infrared wavelength band
OCT	Optical coherence tomography
PD	Polarized dermatoscopy
R	Red wavelength band
SD	Standard deviation
SK	Seborrheic keratosis
SSM	Superficial spreading melanoma

DOI:10.14753/SE.2022.2739

Abstract

Introduction: Melanoma is a melanocytic tumor that is responsible for the majority of skin cancer-related deaths. Breslow thickness is a major prognostic factor for melanoma which is based on histopathological evaluation. Seborrheic keratosis (SK) is a very common benign lesion with a clinical picture that may resemble melanoma.

Materials & methods: We used a multispectral imaging (MSI) LED-based device to distinguish these two entities (melanoma and SK), with the use of autofluorescence imaging with 405 nm and diffuse reflectance imaging with 525 and 660 narrow-band illumination. We analyzed intensity values and shape descriptors of the acquired images. The patterns of the lesions were also assessed with the use of particle analysis. In this work, we assessed also the efficacy of MSI to predict Breslow thickness and developed a classification algorithm to determine optimal safety margins of the melanoma excision.

Results: We found significantly higher intensity values in SKs compared with melanomas and we found a significantly higher number of particles with high fluorescence in SKs. We formulated a parameter, the SK index, using these values to differentiate melanoma from SK with a sensitivity of 91.9% and specificity of 57.0%. We have categorized melanomas into three different subgroups based on Breslow thickness (≤1 mm, 1–2 mm and >2 mm) using our algorithm with a sensitivity of 78.00% and specificity of 89.00% and a substantial agreement ($\kappa = 0.67$; 95% CI, 0.58–0.76). We compared our results to the performance of dermatologists and our algorithm could reach higher sensitivities and specificities.

Discussion & summary: To conclude this imaging technique is potentially applicable to distinguish melanoma from SK based on the analysis of various quantitative parameters. For this application, multispectral imaging could be used as a screening tool by general physicians and non-experts in the everyday practice. In summary based on our findings, this novel method may help also to predict the appropriate safety margins for curative melanoma excision

DOI:10.14753/SE.2022.2739

1. Introduction

1.2. Malignant melanoma

Melanoma (malignant melanoma, MM) is a malignant tumor that arises from melanocytes. It is responsible for the majority of skin cancer-related deaths (1, 2). Worldwide, approximately 232,100 new patients are diagnosed with melanoma annually and it accounts for about 55,000 deaths every year (3). Today, MM is considered a multifactorial disease with genetic factors and environmental influences, where the most important and potentially modifiable environmental risk factor is exposure to ultraviolet (UV) rays, which have genotoxic effects (4). *Gandini et al* have studied the association between MM and solar radiation, concluding that the intermittent UV exposure appears to be the major factor in the development of MM (5). Multiple severe sunburns in childhood or adolescence are particularly harmful (6). Fitzpatrick I and II skin types, red and blonde hair colour, freckles, and light eye colour are considered predisposing factors (7). High numbers of pigmented naevus, as well as atypical and congenital pigmented moles, are also a risk factor (8, 9). However, only 30% of melanomas develop at the base of naevus, they develop mostly *de novo*, in intact skin (10). Various genetic factors, such as CDKN2A or BRAF mutations, as well as immunosuppressed status, are also a significant risk factor (11).

Melanoma has four main subtypes: superficial spreading melanoma (SSM), nodular melanoma (NM), lentigo maligna melanoma (LMM), and acral lentiginous melanoma (ALM). Rare variants, such as desmoplastic melanoma, amelanotic melanoma, uveal melanoma and mucosal melanoma (12-14) (Figure 1.). Unlike other types of skin cancers, melanoma bears with an extreme metastatic potential and thus mortality, when compared to the total tumor burden. This is why early diagnosis and treatment is crucial for the patients' long-term survival. Despite the easy accessibility, the differential diagnosis of melanoma is still challenging. The dermatoscopic picture of MM is characterized by an irregular pigment network that breaks without transition to the periphery, areas of different colored unstructured areas, and diverse pigment clumps, often irregularly located at the periphery of the tumor. The bizarre vascular pattern, the opalescent red

clots, are also characteristic of melanoma. Bluish-grey dots (in melanomas with spontaneous regression) may also be present, but are not of diagnostic value, as they may be present in other lesions (15). There are many skin disorders which are similar to melanoma, including dysplastic nevus, lentigo maligna, congenital and acquired pigmented nevus, non-melanoma skin cancers, Bowen's disease, actinic keratosis, Spitz-nevus, blue nevus, hemorrhage, seborrheic keratosis and others (16-21). There is a subgroup of malignant melanomas that are so similar to SKs that they make up even a new entity named SK-like malignant melanomas (22). According to the American Academy of Dermatology, the National Institute of Health and the National Comprehensive Cancer Network, histopathological evaluation after surgical removal is the gold standard for the diagnosis of melanoma (23, 24). The treatment for primary malignant melanomas is surgical excision with an appropriate safety margin. In certain countries it is done as a two-step procedure when the primary resection is followed by a re-excision after the histopathological definition of the tumor thickness (25). Melanoma in the early stages can be treated successfully with surgery alone (26) where advanced cases need more complex treatment (26, 27).

1.1 Histopathological evaluation of melanoma and Breslow thickness

The Breslow tumor thickness or Breslow thickness is the maximum invasion depth of the melanoma, the distance is given in millimeters between the granular layer of the epidermis or the base of ulceration, and the deepest point invaded by tumor cells (23, 28) not including deeper follicular or adventitial extension (23). This is a vital element of the tumor staging (29) which defines the required surgical safety margin (30) (Table 1). Reoperation is needed if histology finds thicker melanoma than clinically expected and the melanoma excision had insufficient surgical margins. On the other hand, when the tumor thickness is overestimated, a larger scar and potential loss of function of the affected area can cause an unwanted burden for the patients (31, 32). The treatment of melanomas in the head and neck area was proven to be even more challenging, and excision with an appropriate surgical border is not always possible because of the proximity of vital structures (33).

Table 1. Surgical margin recommendations for primary cutaneous melanoma (28)

Tumor thickness	Surgical margin*
In situ	0.5 cm †
≤1.0 mm	1 cm
1.0 to 2.0 mm	1-2 cm
>2.0 mm	2 cm

*** Surgical margins are measured from the border of the lesion clinically at the time of surgery or biopsy. Margins may be modified depending on the site or because of functional considerations.**

† 1 cm margin may be needed for lentigo maligna type *in situ* melanomas, especially larger lesions on the facial region.

Breslow thickness is also the strongest predictor of metastatic spread (33) and determines the need for sentinel lymph node biopsy (SLNB). According to the current guidelines, SLNB is required if Breslow thickness is more than 0.8 mm (34). The US and the European approach to surgery somewhat differ when the Americans tend to biopsy every melanoma to determine the proper safety margin and then perform resection according to the histopathology measurements (35). Europeans often make a clinical assessment of the tumor depth and remove the melanoma with the presumed safety margin in just one step and only make a second surgery when the first assessment was incorrect (36, 37). To reduce the number of surgical intervention and increase tumor depth assessment accuracy, optical imaging modalities have a great potential in the diagnostics of melanoma. Compared to other malignancies, the visibility and easy accessibility of melanoma creates an opportunity for various imaging modalities and screening methods. Early diagnosis is the most important factor in the successful management of melanoma (38, 39), where imaging modalities play a crucial role. Certain imaging methods have been used to analyze the thickness of melanoma beyond histology, such as dermatoscopy (40), high-resolution ultrasound (41), confocal laser-scanning microscopy (42) and photoacoustic microscopy (43).

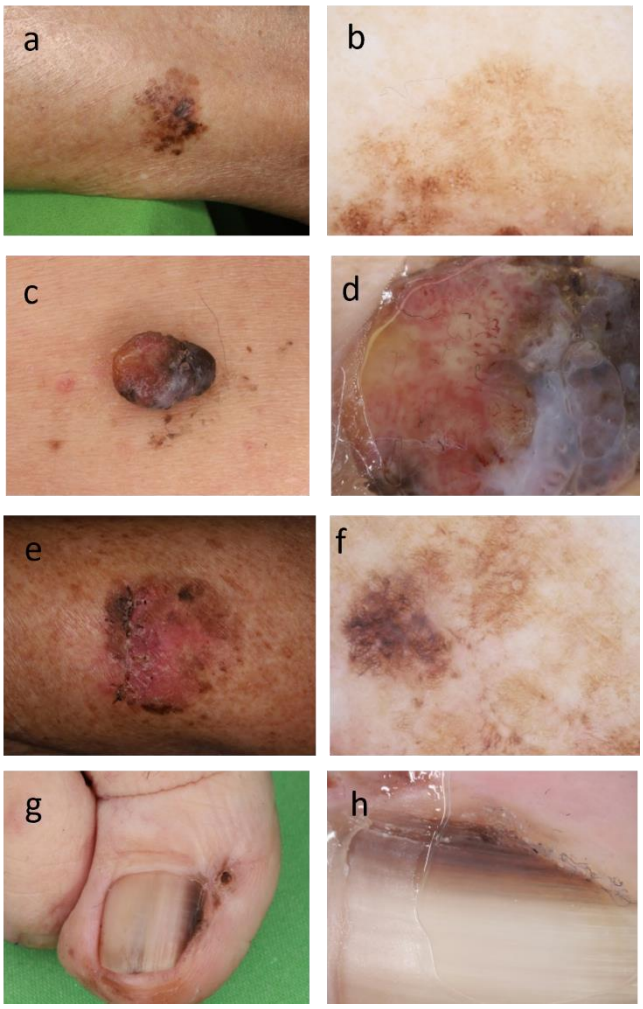

Figure 1. The four main subtypes of melanoma; Superficial spreading melanoma (SSM), Clark II, Breslow tumor depth: 0.345 mm, pT1a, clinical picture (a) and dermoscopic picture (b). Nodular melanoma (NM), Clark IV, Breslow tumor depth: 4.3 mm pT4b clinical picture (c) and dermoscopic picture (d). Lentigo maligna melanoma (LMM), Clark II, Breslow: 0.66 mm pT1a, clinical picture (e) and dermoscopic picture (f). Acral lentiginous melanoma (ALM), Clark II, Breslow tumor depth: 0.37 pT1a clinical picture (g) and dermoscopic picture (h). Clinical and dermoscopic images were taken at the Department of Dermatology, Venereology and Dermatooncology. Black markers (area: 0.125 cm2) were used for image alignment.

1.3. Seborrheic keratosis

Seborrheic keratosis (SK) is a common benign epithelial skin lesion which is very frequent among the elderly. In certain cases, when a younger patient is affected, and the

number of simultaneous lesions is low, diagnostic challenges are more likely to occur (44-46). Clinically, early lesions emerge most often from solar lentigines, which are oval, light-to dark brown macules, with sharply demarcated borders. Advanced SKs transform into plaques and have a typical stuck-on appearance (47). Their clinical appearance is often hyperkeratotic, and increased melanin is common (48) (Figure 2.). The dermoscopic criteria for SK is the presence of multiple orange clod, multiple white clods, sharply demarcated border over total periphery and the pattern of thick, curved lines (49). These findings are histologically seen in the papillomatous epidermis, pseudo-horn or milia-like cysts, enlarged dermal capillaries and intraepidermal cysts (50, 51). Comedo-like openings are keratin-filled invaginations of the epidermis whereas milia-like cysts are intraepidermal keratin pseudocysts with a whitish-yellow appearance under NPD (50, 51).

The diagnosis of SK is often made clinically prior to surgery, while skin biopsy or diagnostic excision is reserved for ambiguous cases (22, 44). It is not malignant and its appearance can be cosmetically disturbing [7]. There are different treatment modalities available for the removal of SK. The most appropriate treatment depends on the size and thickness of the lesion, the patient's skin type, the clinical suspicion of malignancy and the clinical experience of the physician. The most common and easily available treatment for SK is cryotherapy. Other options include shave excision, electrocautery and laser treatment. The efficacy of different types of topical agents is also being investigated: these studies have used gels and creams (e.g. tazarotene, imiquimod cream, alpha-hydroxy acids and urea ointment) and vitamin-D analogues (tacalcitol, calcipotriol) to treat hyperkeratotic skin conditions (52).

There is a subgroup of melanomas that appear very similar to SKs and as a new entity which is recently referred to as SK-like melanoma (22). They cannot be distinguished from SKs with the naked eye nor with DS (53). Among SKs there is also a subgroup, the MM-like SKs, which can only be differentiated by using DS.

1.4. Dermoscopy

Dermoscopy (dermatoscopy, DS) is the most widely used imaging modality in dermatology. The dermoscope is an epiluminescence microscope that typically uses a 10x

magnification to give a more detailed structure of a skin lesion (54, 55). Dermoscopes are relatively cheap and widely available tools in the routine clinical practice (16, 56), however, they require special training and expertise, and are not widely used among general physicians Classically it is non-polarized (NPD) and needs immersion medium between the lens and the skin, but the new generation DSs use polarized light (PD) and do not need immersion (57, 58). Both have their advantages and disadvantages, the NPD is suitable to examine the superficial structures, like the horn pseudocysts in seborrheic keratosis whereas the PD can better analyze the deeper features of the skin, including pigment network, pigment globules and vascular structures (59). The digital dermoscope or video dermoscope is feasible since modestly priced miniature cameras became commercially available. Video dermoscopes are capable of acquiring images with greater magnification from the skin and store them on a computer, which is quite beneficial in the practice because the lesions are comparable over time (60). The image processing uses mathematical algorithms to separate the malign lesions from the pigmented moles based on their texture features (17). Full body examination using dermoscopy is time consuming, and it may prove to be difficult to detect melanoma among a high number of other lesions, such as seborrheic keratoses (Fig. 1.) (61, 62). The most recent and widely applied DS algorithm for pigmented skin lesions is the ‘Chaos and clues’ revised pattern analysis. ‘Chaos’ refers to the presence of dermoscopic asymmetry of the pattern, diversity of colors and border irregularity. If chaos is present, we examine the lesion for the nine possible clues for malignancy. The clue patterns are the grey or blue structures, eccentric structureless area, thick lines (reticular or branched), peripheral black dots or clods, lines radial or pseudopods, white lines, polymorphous vessels, parallel lines/ridges, or polygons. Intervention is needed, if the lesion shows changes over time on an adult (49). Dermoscopy is also being used routinely to predict Breslow thickness (63). Specific dermoscopic patterns can be helpful in predicting thickness, such as light brown color, atypical pigment network, regression, and hypopigmented areas which are typical for thinner melanomas. In contrast, thick melanomas are characterized by blue-white veil, milky red areas, blue-black pigmentation, irregular vessels, shiny white streaks, rainbow pattern, ulceration and pseudolacunae (40).

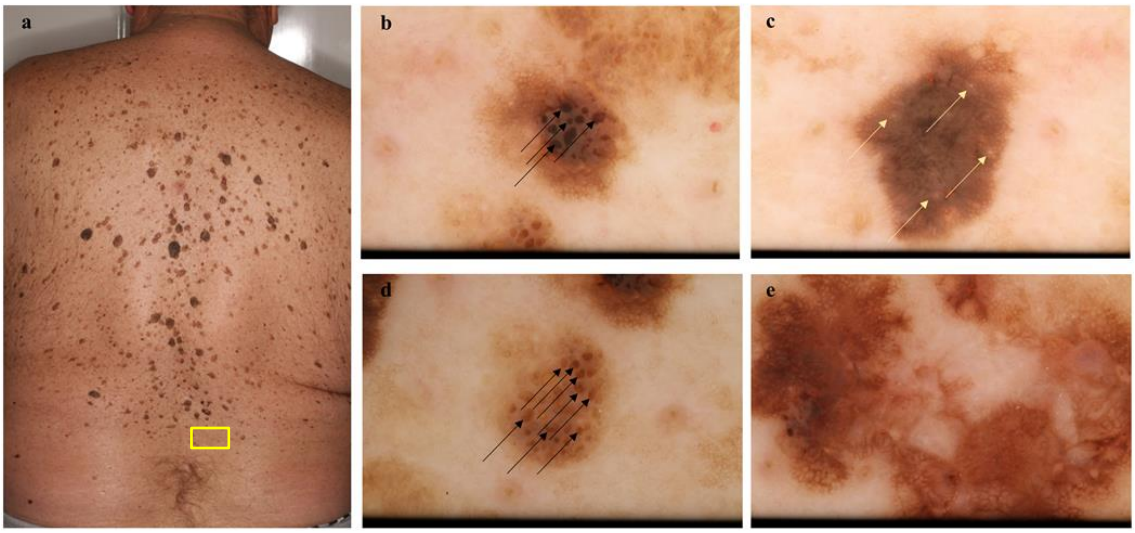

Figure 2. Melanoma among seborrheic keratoses (SK) on the back. This 67-year-old male patient was diagnosed with an *in-situ* melanoma on his back on his lumbal region (yellow rectangle) among many SK lesions(a). Non-polarized dermoscopic images of SKs (b-d) and melanoma (e). SKs (b-d) show a dull surface, including fingerprint and cerebriform patterns, milia-like cyst (yellow arrows) and comedo-like opening (black arrows). Melanoma (e) contains an irregular pigment network and blue-white veil with multiple colors. Non-polarized dermoscopy (NPD) is better for the evaluation of seborrheic keratosis as it visualizes milia-like cysts and comedo-like openings more clearly (64).

1.5. Multispectral imaging

Multispectral imaging (MSI) is an emerging diagnostic tool to detect skin cancer *in vivo*. MSI utilizes different wavelength bands, mostly the visible and the infrared spectrum of the light (400-970 nm), to acquire images of the skin (65) where the light source is usually provided by halogen lamps or LEDs (66). During MSI, a set of images is taken from the same skin location with the use of different wavelength bands (67). This method combines the advantages of spectrophotometry (spectral resolution) and digital cameras (spatial resolution) (68). MSI has been used earlier to map skin chromophores such as hemoglobin and melanin for direct and noninvasive skin assessment (69). The primary advantage of MSI compared to other imaging modalities is its cost-effectiveness and the possibility of implementation into smartphone cameras (70, 71), that renders this technique easily accessible (70, 71). The use of MSI in the field of dermatology has been emerging in the last twenty years. A LED-based MSI device was recently successfully introduced for the detection recurring skin cancers (32, 72) and proved to be applicable

in the differentiation of different tumor types from benign lesions based on their mean intensity of autofluorescence (AF) (73). In addition, MSI has been also utilized for the detection of rare skin disorders (74) (75) (Figure 3.).

Multispectral imaging tools that have been adopted as diagnostic aids in the evaluation of skin lesions are the SIAscope, FotoFinder and Verisante Aura (76). The SIAscope emits radiation at wavelengths between 400 and 1000 nm and produces eight narrow-band spectrally filtered images. This technique can be used to examine the vascularity, pigment network and collagen content of the lesion. However, its sensitivity and specificity is lower compared to dermatoscopy (77).

MoleMate is a computerised tool combining SIAscope technology and a scoring algorithm. It aims to facilitate the detection of suspicious lesions and referral to an expert in primary care. In a randomised trial, the proportion of lesions treated appropriately was similar between primary care physicians using only clinical criteria (history, physical examination) and those who also used MoleMate (78).

A Canadian prospective study compared the diagnostic accuracy of dermatologists' physical examination, teledermatoscopy and four image analysis systems (MelaFind, FotoFinder, FotoFinder Moleanalyzer Pro and Verisante Aura) for 209 skin lesions in 180 patients, including biopsy and histopathology. Using histopathological diagnosis as a reference, the sensitivity and specificity of the automated systems were 82.5% and 52.4% for MelaFind, respectively; 83.1% and 75.2% for FotoFinder ; 88.1% and 78.8% using FotoFinder Moleanalyzer Pro, respectively; and 21.4% and 86.2% for Verisante Aura, respectively. The sensitivity and specificity of the teledermatoscope were 84.5% and 82.6%, respectively, while the physical examination of dermatologists showed these characteristics to be 96.6% and 32.2%, respectively (79).

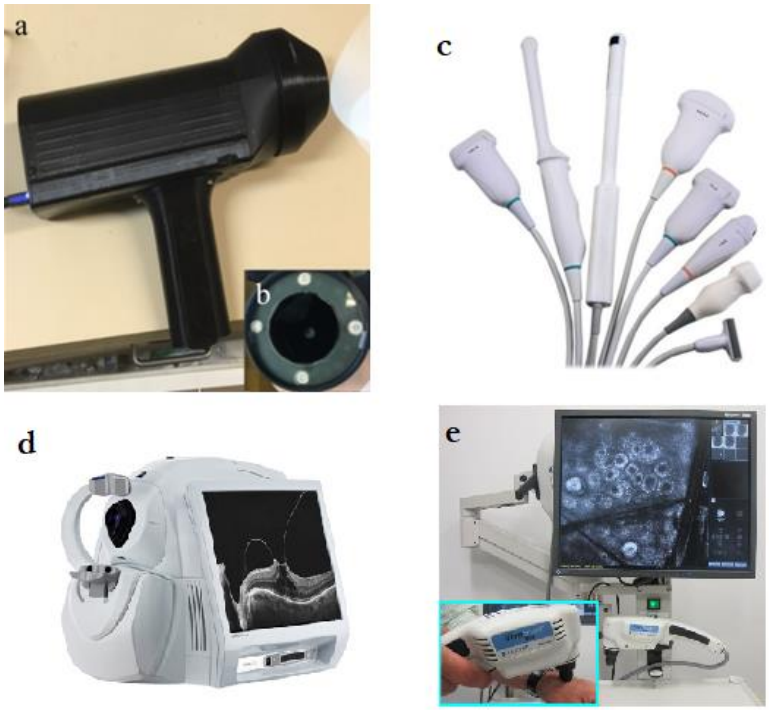

Figure 3. Imaging modalities: Multrispectral Imaging prototype used in this study (a) and its LED-ring (b)., High Frequency ultrasound transducers (image source: https://www.visualsonics.com/product/transducers) (c) Optical coherence tomography (CIRRUS HD-OCT 5000 image source: https://www.ophthalmologyweb.com/Retina/5458-Optical-Coherence-Tomography-OCT/) (d) Vivascope Reflectance Confocal Microscope System - (handheld Vivascope 3000 image source: https://www.researchgate.net/figure/Vivascope-Reflectance-Confocal-Microscope-System-Inset-shows-the-handheld-Vivascope-3000_fig1_279635544) (e)

1.6. Other imaging modalities used in melanoma diagnosis and depth measurement

Optical imaging modalities have great potential in melanoma diagnosis. Certain imaging methods have been used to assess melanoma thickness, such as high-frequency ultrasound (HFUS) (41), optical coherence tomography (80) or confocal microscopy (81, 82).

High-resolution ultrasound at 5-18 MHz is widely used for imaging in clinical medicine. The use of high-frequency ultrasound (HFUS) between 20 and 100 MHz increases resolution and is therefore a well-suited method for the investigation of inflammatory skin diseases, oedemas and tumours (83). The most commonly used frequency around 20 MHz allows good separation of skin layers, with a penetration depth

of 6-7 mm and a resolution of 50-200 μm. HFUS is very effective for assessing the depth of spread in basal cell carcinomas and for monitoring treatment in conservative therapies. In cases of hidradenitis suppurativa, HFUS can also aid staging. Skin ultrasound has the advantage of being a safe, cost-effective and reproducible imaging modality. The disadvantage of HFUS is that its accuracy is highly dependent on the skill of the examiner. Furthermore, many lesions may show similar ultrasound images and are therefore better used in combination with other methods with higher resolution. The High-frequency ultrasound (HFUS) is mainly used in dermatology to quantify the physiological and anatomical changes of the dermis including vascularization and thickness (84). But it also proved to be a useful modality to evaluate the type and degree of infiltration of basal cell carcinomas (85). It is also being used for staging hidradenitis suppurativa (86). Recently, the presurgical measurement of tumor depth using HFUS became considerable after some authors reported their successful use (25, 87), but it is still far from the general use in the everyday practice (Figure 3.)

Optical coherence tomography (OCT) is an optical reflectance-based tool that uses low-coherence light to penetrate into the skin. It has been widely used in the ophthalmology for many years to visualize the retina (80). OCT is a non-invasive, real-time, optical imaging technique based on the interference of infrared radiation with living tissue in vivo. OCT enables high-resolution, two- or three-dimensional cross-sectional imaging of tissue microstructural morphology (88). It is increasingly popular in dermatology and proved to be applicable in the diagnosis of basal cell cancer and actinic keratosis (80). OCT can be used to diagnose MM and non-melanoma skin tumors and to define the tumor borders. It can also be used to monitor the status of inflammatory skin diseases and to assess skin ageing caused by photodamage. The disadvantages are that the quality of the images is highly dependent on the experience of the examiner and that no information about cellular structures can be obtained (89) (Figure 3.).

In vivo reflectance confocal microscopy (RCM) is a novel imaging technique in dermatology used to detect dermato-oncological cancers with promising results. It uses near-infrared light from diode laser to detect the differences between the reflectance characteristics in the tissue (81). Confocal microscopy contain a light source, condenser, collimator, ever-changing objective lens and detector. The examination requires the probe

head containing the objective lens to be in contact with the skin and the application of an appropriate immersion medium. The instrument emits near-infrared light that reflects off epidermal structures to produce a three-dimensional image at 30x magnification. Melanin granules have a high refractive index and therefore reflect more light. This allows the RCM image to show areas with high melanin content more clearly (90). The disadvantages of RCM are high cost, limited availability and longer scan time (about seven minutes/lesion) (91). and can differentiate between the melanoma and other equivocal melanocytic lesions (82). However, these are very expensive devices, their use requires special skills and their availability is generally limited to large dermatology centers (65, 92) (Figure 3.).

Teledermatology is the most expanding field for low-cost, home use imaging in dermatology, when the patients are the users and the subjects of the imaging at the same time. There is an emerging number of new applications and their performance improves constantly, which will consequently lead to a wider acceptance (93, 94). During the COVID-19 pandemic teledermatology was also an aiding tool to reduce the number doctor’s visits and reduce the need for hospital visits while it keeps the diagnostic accuracy (94). Teledermatology has evolved significantly in the past decade, but the accuracy of face-to-face dermatology is still higher than the teledermatology which cannot be replaced, yet (93).

2. Objectives

The aim of the present study was to investigate spectral reflectance and autofluorescence properties of melanoma to achieve 2 main goals:

1) Estimate the depth of melanomas with the help of an MSI based device using G, R and IR light and compare it to the performance of clinical assessment by dermatologists and dermatology residents. The detailed description of this prototype device was previously published (92, 95). We have measured the mean gray value (integrated density/area), circularity(4π*area/perimeter^2), solidity (area/convex area) and roundness (4*area/(π*major_axis^2)) (Figure 4.). An additional first step was built in in this algorithm to rule out pigmented nevi using parameter *s'* (Equation 1) based on our previous studies (96-99). The LED-based multispectral images were analysed with ImageJ v1.46 software (NIH, Bethesda, MD, USA) (100).

$$parameter\ s' = lg \frac{I_G \cdot I_{R_{skin}}^2}{I_{G\_skin} \cdot I_{R\_skin}^2} \quad (1)$$

where I_G : intensity of lesion in green channel,

I_G _skin: mean intensity of skin in green channel,

I_R : intensity of lesion in red channel,

I_{R_skin} : mean intensity of skin in red channel.

DOI:10.14753/SE.2022.2739

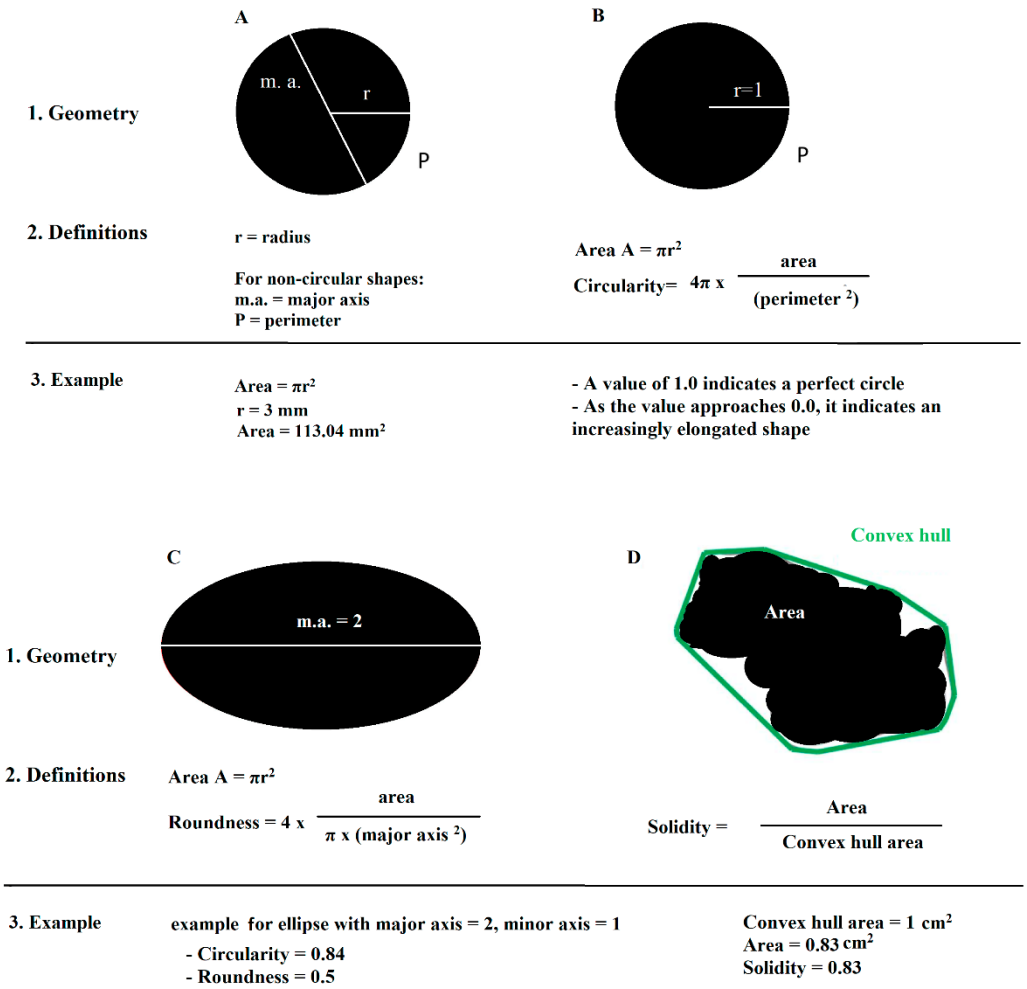

Figure 4. Shape descriptors and their mathematical definitions (101, 102). By definition a circle is a plain shape consisting of all points that are at a given distance from a given point, the centre and the distance between any point of the circle and the centre is called the radius (A). The circularity is a shape descriptor which is the function of the area of the circle and the perimeter (101). A value of 1.0 indicates a perfect circle (B). The roundness is defined as a function of the area and the length of the major axis(C) (101) whereas the solidity is the ratio of the area and the convex hull area (D)(102).

2) Our second aim was to compare the MSI characteristics of melanomas to seborrheic keratoses to distinguish these two entities using a novel MSI based index operating with AF, G and R light, the SK index (Equation 2). For the intensity analysis we manually selected the skin lesions ROI using the AF, G and R channels. We analyzed the intensity including minimum and maximum, mean intensity value and standard deviation (SD), to compare melanomas with SKs regarding these parameters. We calculated ratios of the intensity values of the different channels including AF, G and R and used these ratios (AF/G, AF/R) to differentiate melanomas from SKs. We also measured the ratio of the pixels with the lowest and highest intensity values within each lesion (Min/Max). During this comparison we focused more on the more challenging lesions including melanoma (MM)-like SKs and SK-like MMs. Academic literature will be drawn upon to discuss these findings and the paper will close with recommendations for applications in the everyday practice. The LED-based multispectral images were analyzed with ImageJ v1.46 software (NIH, Bethesda, MD, USA) [76].

$$SK\ index = \frac{2 \cdot AF \cdot StDev \cdot (\frac{Min}{Max})}{G \cdot R} + (Particle\ number \cdot Area\ \%) \quad (2)$$

DOI:10.14753/SE.2022.2739

3. Results

3.1. Melanoma tumor depth analysis

3.1.1. Patient data and histology

In the melanoma tumor depth analysis, we have examined one hundred patients with primary melanoma of the skin. In total, we have collected 128 image sets. Of the 100 melanomas, 69 were SSM (69%), 19 NM (19%), 2 ALM (2%), 3 LMM (3%), 1 naevoid (1%) and 6 unclassified (6 %). The mean age of melanoma patients was 62.64 ±14.29 years. The sex ratio of the affected patients was 37% women and 63% men. The mean Breslow tumor thickness was 1.777 ±1.728 mm, ranging from 0.12 mm to 7.5 mm (Figure 5).

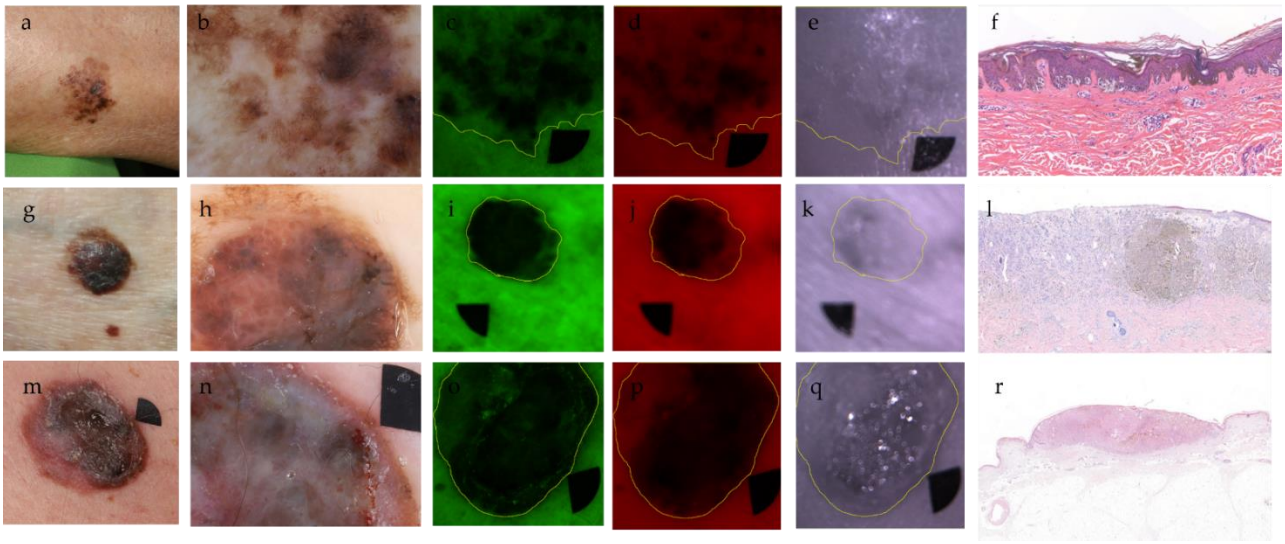

Figure 5. Melanomas with different Breslow thicknesses, Upper row (a-f); Melanoma with Breslow 0.345 mm, pT1a, Clark II, superficial spreading melanoma (SSM), clinical photograph (a), dermoscopic image (b), G (c), R (d) and IR (e) channels and histological image (f). Middle row (g-l); Melanoma with Breslow 1.81 mm, pT2a, Clark IV., SSM, clinical photograph (g), dermoscopic image (h), G (i), R (j) and IR (k) channel, histological image(l) Lower row (m-r); Melanoma with Breslow 2.42 mm, pT3b, Clark IV., SSM with a nodular component, clinical photograph(m), dermoscopic image (n), G (o), R (p) and IR (q) channels and histological image (r). Black markers (area: 0.125 cm^2) are used for image alignment. Histology magnification 51X (a) and 50X (b,c) (H&E staining).

3.1.2. Intensity values

When the intensity values of various melanomas with different tumor depths were studied, we found significant differences in the green (G) and red (R) MSI channels that allowed us to efficiently differentiate the Breslow≤1 mm subgroup from the other two groups, the Breslow: 1-2 mm and the Breslow> 2 mm subgroups. In these tumors the intensity measured in these channels of Breslow≤1 mm melanomas were significantly higher than in the other two subgroups. IR channel could distinguish between Breslow 1–2 mm melanomas and melanomas with higher than 2 mm Breslow thickness. The other G and R channels allow exclusively to differentiate the more superficial group Breslow≤1 mm from the other more invasive two groups. In summary, the strongest correlation was between IR intensity and Breslow thickness (r: -0.6593, p value: <0.0001, 95% confidence interval: -0.7576 to -0.5317, whereas the G and R channels displayed a lower correlation with tumor thickness (Figure 6).

3.1.3. Shape descriptors

Among the shape descriptors, both circularity and solidity proved significantly lower in the Breslow≤1 mm subgroup than in the other two subgroups. Investigations of the circularity and solidity made it possible to distinguish between the Breslow: 1-2 mm and the Breslow> 2 mm subgroups. This was since Breslow> 2 mm melanomas had significantly higher circularity and solidity values. At the same time the roundness did not show any significant differences. Circularity (p:<0.0001) and solidity (p:<0.0001) proved to be efficient in differentiating these two groups. Pearson's correlation showed high correlation between solidity (r: 0.6324, 95% confidence interval: 0.4978 to 0.7372, p: <0.0001) and between circularity and Breslow thickness (r: 0.7109 95% confidence interval: 0.5980 to 0.7961, p: <0.0001) whereas the roundness showed no significant differences between the three subgroups (p value=0.2139) (Figure 6).

3.1.4. Differentiation nevi from melanomas with the use of parameter *s'*

We used the patient data of the melanoma patients mentioned before of the Department of Dermatology, Venereology and Dermatooncology, Semmelweis University (Budapest, Hungary) from which 98 patients met the requirement of the

parameter s' assessment (126 image sets). We used the patient date of the Oncology Centre of Latvia (Riga, Latvia) including 143 nevi (143 image sets). The acquired images were automatically transferred to a cloud server for further data processing and analysis. Parameter *s'* was able to distinguish melanomas from nevi with a sensitivity of 89.60% and specificity of 88.11% as the first step of the algorithm (n= 98 MMs and 143 nevi). The melanomas had significantly higher parameter *s'* values compared to the nevi. The ROC AUC analysis also showed significant differences. The comparison of melanoma and nevus groups had an AUC of 0.944 (patients: melanoma, control: nevi, 95% confidence interval, p<0,0001) (Figure 7).

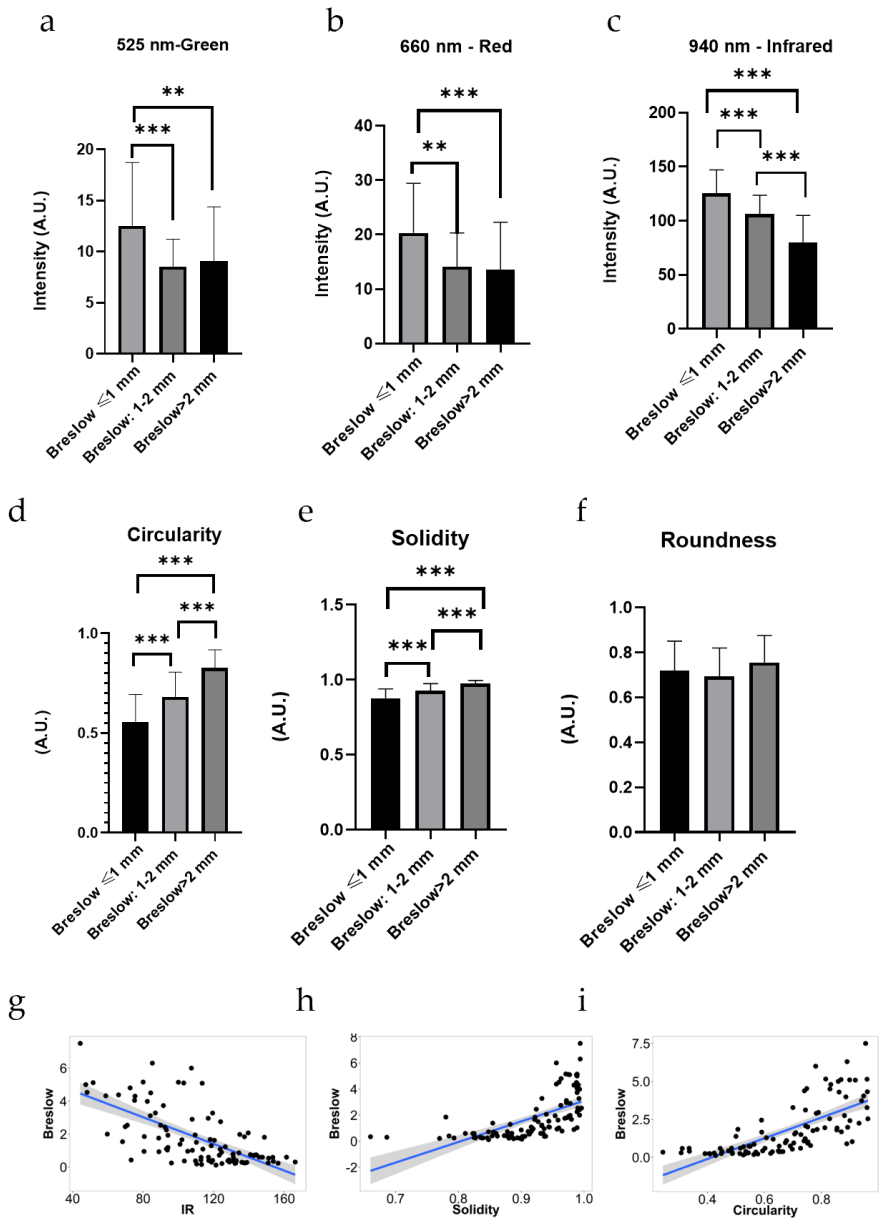

Figure 6. Melanoma comparison having different tumor thicknesses and correlations between intensity values, shape descriptors and Breslow thickness. One-way ANOVAs and Tukey's post comparison tests were used to compare the intensity values and shape descriptors. The intensity values proved to be statistically significant (a) G ($p<0.0001$), (b) R ($p<0.0001$) and (c) IR ($p<0.0001$) and among the shape descriptors (d) Circularity ($p<0.0001$) and (e) Solidity ($p<0.0001$) were found statistically significant. The roundness (f) was not able to separate the three groups effectively (p: 0.2759). Moreover, the (G (a), R (b), and IR (c) channels proved to be effective to identify tumors of Breslow≤1 mm from the other two groups, whereas the IR channel could differentiate the Breslow: 1-2 mm and Breslow>2 mm form each other. Pearson's correlations were used to correlate the Breslow thicknesses with IR channel values, Circularity and Solidity. The correlation was high between IR intensity (g) and Breslow tumor thickness (r: -0.659, 95% confidence interval: -

0.7576 to -0.5317, p: <0.0001), whereas the correlations between Breslow tumor thickness and G or R intensities were low (r: -0.226 and -0.244, respectively). The correlation was high between solidity and Breslow thickness (h) (r: 0.6324 95% confidence interval: 0.4978 to 0-7372, p: <0.0001) and high between circularity and Breslow thickness (i) (r: 0.7109, 95% confidence interval: 0.5980 to 0.7961, p: <0.0001) P values below 0.05 were considered statistically significant. The results are expressed as mean ± standard error (n=100). A.U.= Arbitrary unit.

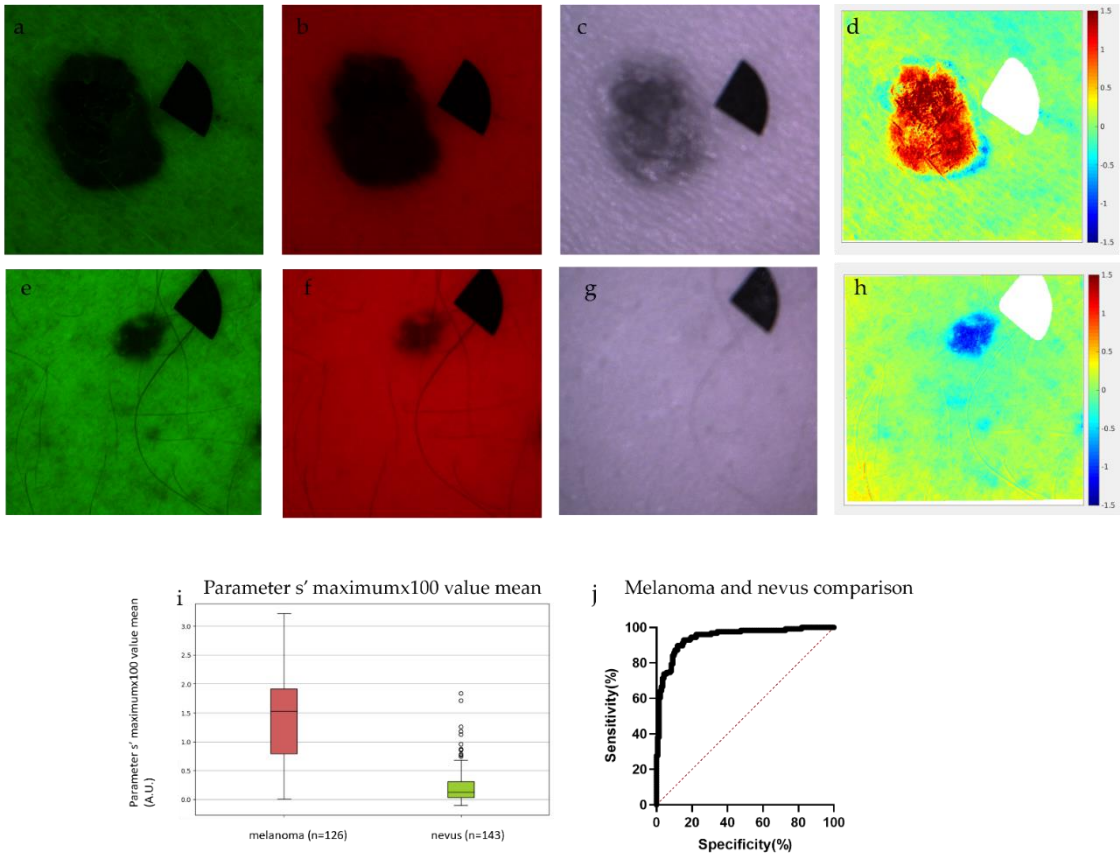

Figure 7. Differentiation of nevi from melanomas with the use of parameter *s'*. A superficial spreading melanoma, Breslow: 1.02, Clark: IV., pT2a (upper row) and a pigmented nevus (middle row). The parameter maps (d,h) were calculated using the G (a,e), R (b,f) and IR (c,g) channels. The melanoma with higher parameter *s'* is red (d) whereas the nevus with its lower parameter *s'* is visualized deep blue (h). The redness means higher probability of melanoma (highest parameter *s'* is 1.5 :rufous color) while blueness refers to a higher probability of nevus (lowest parameter *s'* is -1.5: deep blue color). (Using the maximum values (i) with a threshold of 0.511 arbitrary unit (A.U.) melanomas could be differentiated from nevi with a sensitivity of 89.60% and specificity 88.11%. The Area Under the Curve (AUC) was 0.944 (patients: melanoma, control: nevi, 95% confidence interval, p<0,0001) (j). Y-axis: sensitivity, x-axis: 1-specificity. Black markers (area: 0.125 cm2) were used for image alignment.

3.1.5. Melanoma classification algorithm

We have developed a novel MSI-based melanoma classification algorithm based on the shape descriptors and intensity values that allows us to classify melanomas into the above-mentioned three subgroups with a sensitivity of 78% and specificity of 89%, (Figure 8.). The sensitivities for each subgroup were 80.85% (Breslow≤1 mm), 76.19% (Breslow: 1-2 mm) and 81.25% (Breslow>2 mm). The specificities were 96.22% (Breslow≤1 mm), 82.27% (Breslow: 1-2 mm) and 94.11% (Breslow> 2mm). The total agreement for predicting the right subgroup was found substantial (κ = 0.67; 95% CI, 0.58-0.76), also it was substantial classifying melanomas to Breslow≤1 mm subgroup (κ = 0.76; 95% CI, 0.63 to 0.89) and to Breslow>2 mm subgroup (κ = 0.73; 95% CI, 0.59 to 0.88). The agreement was moderate when the algorithm was classifying melanomas to the Breslow: 1-2 mm subgroup (κ = 0.47; 95% CI, 0.28 to 0.65) (Table 2.)

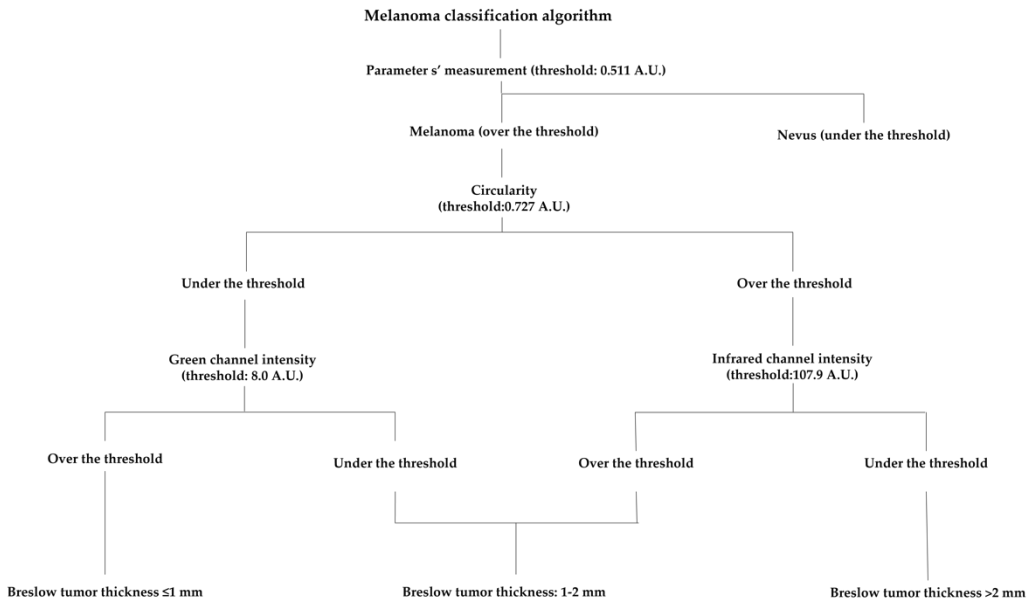

Figure 8. Melanoma classification algorithm tree Based on the shape descriptors and intensity values; our melanoma classification algorithm was calculated to classify the multispectral images of melanomas into three different Breslow tumor thickness subgroups. First step was to establish a threshold between lower and higher circularities (threshold: 0.727 A.U.), which sorted melanomas into two groups: 1) low and 2) high circularity. The second step was sorting melanomas from these 2 subgroups to the three previously defined groups (Breslow tumor thickness≤1 mm, Breslow tumor thickness: 1-2 mm and Breslow tumor thickness>2 mm). We used the intensity values of green channel (threshold: 8.0 A.U.) and the infrared channel (107.9). This algorithm was able to classify melanomas into these three subgroups with a sensitivity of 78% and specificity of 89%.

3.1.6. Dermoscopic photograph analysis by dermatologists and dermatology residents

The total sensitivity of the human expert categorization (n=16 dermatologists and 17 dermatology residents) into the three subgroups described above was 60.38%, while the specificity was 80.86% with a moderate total agreement (κ = 0.41; 95% CI, 0.40 to 0.43), (Table 2.). The sensitivity of the assessment by dermatologists was 62.19% with a specificity 81.09% and a moderate agreement (κ = 0.44; 95% CI, 0.42 to 0.47), where at the same time the sensitivity of the evaluation by dermatology residents was 58.44%, with a specificity of 79.76% and a fair agreement (κ = 0.39; 95% CI, From 0.36 to 0.41). Among the subgroups, classifying into the Breslow>2 mm subgroup had the highest total sensitivity of 90.37% and specificity of 78.58% with high substantial agreement (κ = 0.65; 95% CI, 0.61 to 0.69). Classification into the Breslow≤1 mm subgroup had a sensitivity of 51.69% and specificity of 96.95% with a moderate agreement (κ = 0.49; 95% CI, From 0.46 to 0.52). The classification into the Breslow: 1-2 mm subgroup had a sensitivity of 38.51 % and a specificity of 72.07% without agreement (κ = 0.09; 95% CI, 0.06 to 0.13).

Table 2. Results of the comparison of the melanoma classification algorithm and the assessment based on dermoscopic and clinical images by dermatologist and dermatology residents (n=100)

	Melanoma classification algorithm	Assessment based on dermoscopic and clinical image
Cohen's kappa	0.67	0.41
Sensitivity	78.00%	60.38%
Specificity	89.00%	80.86%

4.2. Differentiating melanoma from seborrheic keratosis

4.2.1. Dermographic data

We have examined total of 266 patients with melanoma or SK and taken one or more image sets of their lesions depending on the lesions' number and size. Many patients

with SKs had several lesions increasing the number of image sets taken. Out of the total 127 patients (161 image sets) were histologically proven melanomas from which 66 were SSM (52 %), 18 NMs (14.1%), 21 in situ melanomas (16.5%), 3 ALM (2.3%), 1 LMM (1%) and 18 unclassified (14.1%). Six patients had SK resembling MMs (6 image sets). Comparison was made to 139 patients (319 SK lesions with 319 image sets) diagnosed with SK by dermatologists (2-3 SKs/patient) with the use of a commercial Heine Delta 20 (HEINE Optotechnik GmbH & Co. KG, Gilching, Germany) dermoscope. 30 patients had MM resembling SKs (52 image sets). The mean age of patients with melanoma and SK was 64.09 ±13.55 and 70.19 ±11.147 years, respectively. The gender ratio was 44 % women and 56 % men among patients with melanoma and 44.9% women and 55.1% men among patients with SK.

4.2.2. Intensity values

In SKs, the AF/G, AF/R and Min/Max ratios proved to be all significantly higher compared to melanomas. Milia-like cysts and comedo-like openings showed very high AF intensities which appeared small and contained dense signals inside the lesion leading to AF inhomogeneity. Disproportions in intensity values of the SK lesions resulted in significantly higher SD compared to melanomas. While milia-like cysts and comedo like openings appeared as bright particles embedded into SK lesions, melanomas did not contain these type of particles (Figure 9.). We analyzed also the challenging cases including the melanoma (MM)-like SKs and SK-like MMs using the same method. In MM-like SKs all the intensity values were similar, yet significantly higher compared to SK-like melanomas including AF/G, AF/R, SD, Min/Max (Figure 10.)

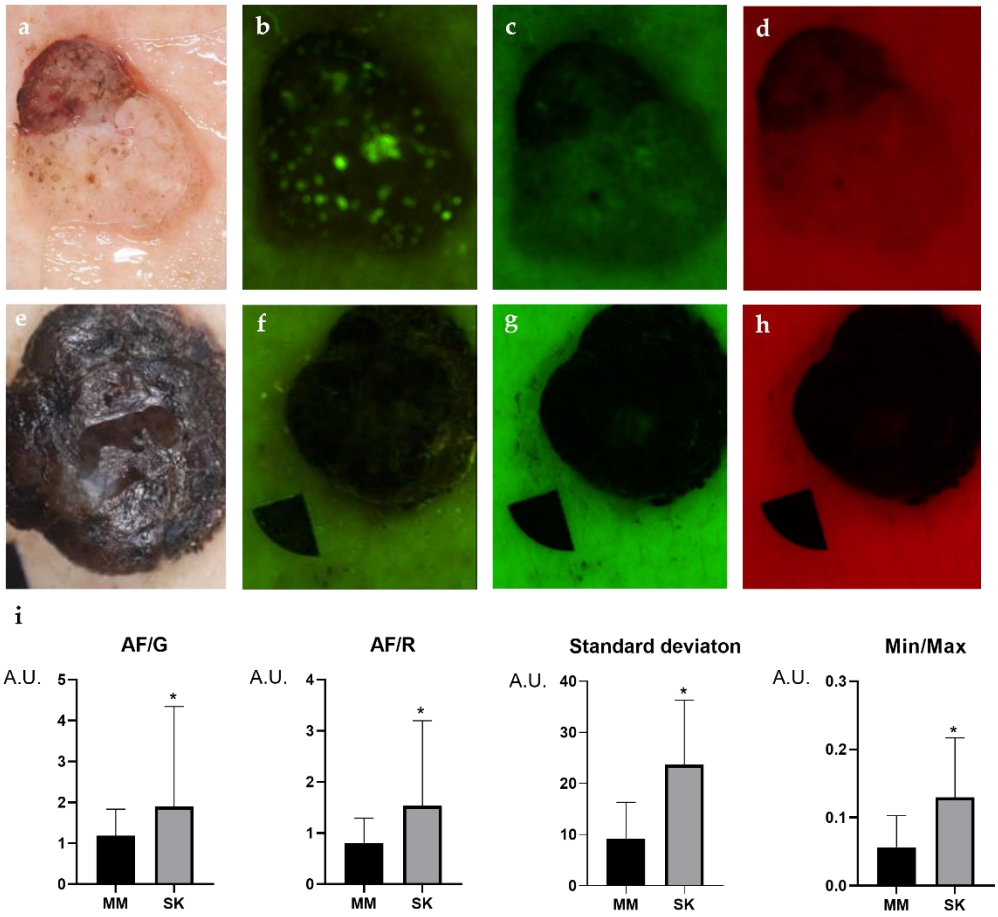

Figure 9. Multispectral LED images comparing a seborrheic keratoses (SKs) (a-d) to melanomas (e-h), and the results of statistical analysis of intensity parameters (i). Dermoscopic images of the lesions (a, e), 405 nm autofluorescence (AF) channel (b, f), 525 nm green (G) (c, g) 660 nm red (R) channel images (d, h). Welch's t-test was used to compare the intensity values of the lesions. In SKs all the intensity values were significantly higher compared to melanomas (i). The AF/G and AF/R ratios were normalized to adjacent control skin. A.U., arbitrary unit. P values below 0.0001 were considered statistically significant. Means ±SD: AF/G: 1.187±0.647(MM) vs. 1.891±2.437 (SK), AF/R: 0.809±0.48 (MM)vs 1.53±0.48(SK), Standard deviation: 9.23±7.1(MM) vs. 23.6±12.58(SK), Min/Max: 0.056±0.045(MM) vs. 0.129±0.087 (SK). Black markers (area: 0.125 cm2) were used for image alignment.

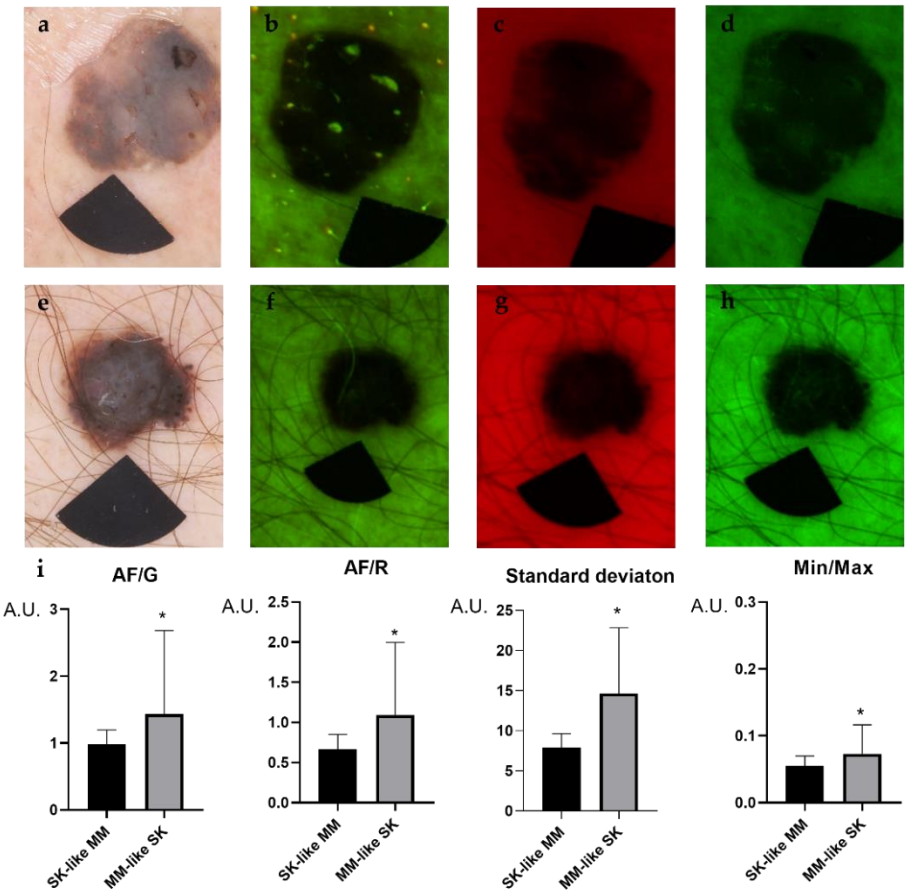

Figure 10. Representative multispectral and dermoscopic images of clinically challenging melanoma (MM)-like SKs and SK-like MMs. The upper row is a SK-mimicking melanoma (MM) (nodular melanoma, Breslow:1.84, Clark III., pT2a) while the lower row is a melanoma-resembling SK. Dermoscopy images of the lesions (a, f), 405 nm autofluorescence (AF) channel (b, g), 660 nm red (R) channel images (c, h) 525 nm green (G) (d, i) and the results of particle analysis (e, j). Welch's t-test was used to compare the intensity values of the lesions. In SKs all the intensity values were significantly higher compared to melanomas (i). A.U., arbitrary unit. P values below 0.05 were considered statistically significant. Means ±SD: AF/G: 0.984±0.212 (SK like MM) vs 1.415±1.215 (MM like SK), AF/R: 0.667±0.183 (SK like MM) vs 1.08±0.884 (MM like SK), Standard deviation: 7.9±1.745 (SK like MM) vs 14.79±7.96 (MM like SK), Min/Max: 0.05±0.01 (SK like MM) vs 0.073±0.043 (MM like SK). Black markers (area: 0.125 cm2) were used for image alignment.

4.2.3. Particle analysis

During the particle analysis melanomas appeared as lesions with homogenous intensity, whereas SKs had many high intensity particles embedded in the lesions, their intensity pattern was heterogenous (Fig. 11.). Our algorithm counted significantly higher number of particles in SKs, which took greater part (Area%) of the lesion (Fig.

11.). We analyzed also melanoma (MM)-like SKs and SK-like MMs using the particle analyzing algorithm and the differences of the number of the particles detected and their area % of the lesions were not significantly different between the two groups using Welch's t-test. (Figure 12.). The percentage of melanomas excluded from the analysis amounted to no more than 5% of the total number of cases.

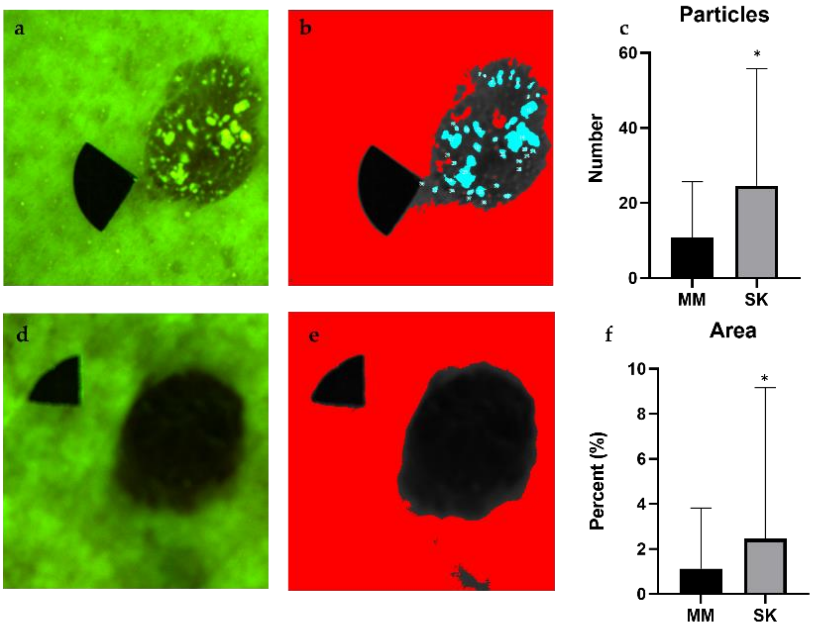

Figure 11. **Particle analysis of SKs (a-b) and melanomas (d-e)** and the results of statistical analysis, including number of particles with high autofluorescence values (c) and the total area of these particles (f). In the ImageJ software we used the Overlay Masks option to visualize the particles (shown in blue color) in these images. Comparing the melanoma values to SK values using Welch's t-test, SKs contained significantly higher number of particles which were also significantly larger (c). The percentage of the area covered by the particles was significantly lower in melanomas compared to SKs (f). The limitations of the algorithm were also visible here, because with these settings not all the particles could be selected and measured (white dots on panel b) P values below 0.0001 were considered statistically significant. Means ±SD: Particles: 10.76±14.9(MM) vs 23.56±30.44 (SK), Area: 1.126±2.698 % (MM) vs 6.412±13.26 % (SK). Black markers (area: 0.125 cm2) were used for image alignment.

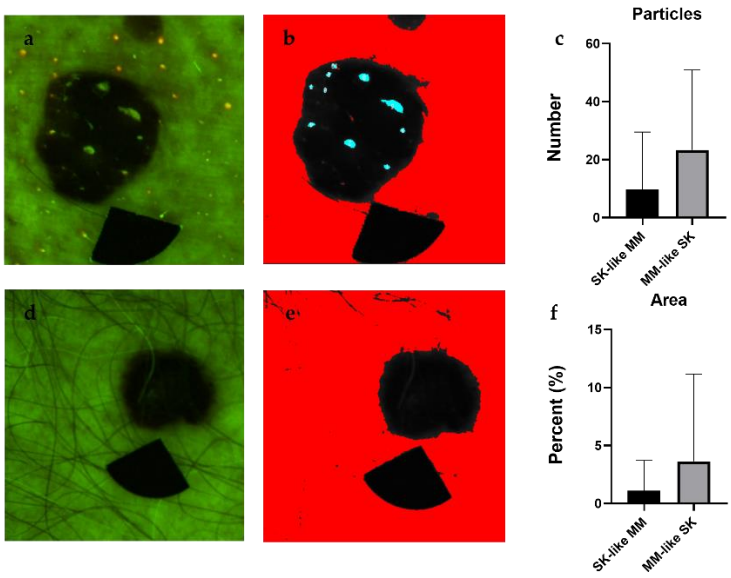

Figure 12. Particle analysis of melanoma (MM) like SKs (a-b) and SK like MMs (d-e) and the results of statistical analysis, including number of particles with high fluorescence values (c) and the total area of these particles (f). We used the Overlay Masks option of the ImageJ software to visualize the particles (shown in blue color) in these images. The differences of the number of the particles detected and their area % of the lesions were not significantly different between the two groups using Welch's t-test. P values below 0.05 were considered statistically significant. Means ±SD: Particles: 9.667±19.87 (SK like MM) vs 22.42±27.10 (MM like SK), Area: 1.11±2.60 % (SK like MM) vs 3.56±7.31 % (MM like SK). Black markers (area: 0.125 cm2) were used for image alignment.

4.2.4. SK index

The sensitivity of the SK index was 91.9 % with a specificity of 57.0 %. The positive predictive value proved to be 51.7% while the negative predictive value was 93.3 %. Among the melanoma-like SKs and SK-like melanomas, the sensitivity was 83.3 %, while the specificity was 51.9 %.

5.Discussion

Innovative technology and new diagnostical techniques emerge daily to penetrate and reform medicine; dermatology is no exception to this trend. In this dissertation we report results of two studies. In the first study our aim was to estimate the Breslow thickness using multispectral imaging. In the second one the goal was to differentiate seborrheic keratosis (SK) from melanoma. In both experimental settings we used the same multispectral imaging (MSI) device but with different wavelength bands and quantitative analyses to create new algorithms to approach these problems. MSI allows the examiner to use different wavelength-dependent features and has been previously used to detect melanomas. Nonetheless, these studies mainly focused on how to differentiate melanomas from other skin lesions (17, 67, 96, 103-105); depth prediction is a field where we lack conclusive research publications (96, 106). To the best of our knowledge, we were the first to analyze melanoma tumor thickness with multispectral imaging to classify melanomas into 3 subgroups of great clinical relevance.

Our first step to improve the algorithm to exclude nevi from the analysis was the introduction of parameter *s'*. Parameter *s'* is an enhanced formula based on our previous findings to differentiate melanoma from nevi (96-99). It uses the intensity values of the lesion and the surrounding skin in G and R channels to calculate a predictive value. In our study, melanomas showed significantly higher parameter *s'* values than nevi. Accordingly, with our thresholding algorithm nevi could be differentiated from melanomas with a sensitivity of 89.60% and specificity of 88.11% (Figure 7.). These data are consistent with the literature where multispectral imaging have been previously applied successfully to differentiate these two entities (17). Apart from multispectral imaging, melanoma and nevus differentiation is one of the most researched topics in dermatology. Many studies have focused on this problem and used computerized and AI-aided methods to differentiate benign lesions from skin cancers (107-111). This is a potentially applicable step to rule-out benign pigmented nevi and reconsider the clinical diagnosis when our algorithm is used to estimate tumor thickness of melanoma.

The second step was based on the measurement of the shape descriptors and intensity values of the lesions. Shape descriptors were capable to differentiate high and low-risk

melanomas, namely over 2mm vs. less than 1 mm. SMMs are more common among thin melanomas (P < .001) and NMs are more common among patients with thick melanomas (P < .001) (112).The combination of shape descriptors and intensity values were sensitive and specific approach was enough for the melanoma classification algorithm to sort melanomas into the three categories with a sensitivity of 78.00 %, specificity of 89.00 % with a substantial agreement (κ = 0.67; 95% CI, 0.58-0.76). Circularity, the sphericity of lesions was the most applicable shape descriptor to classify melanomas into a low- and a high-risk group as the second step. Larger and thicker melanomas were more circular. Roundness showed no significant differences because roundness is less sensitive to variations in perimeter length compared to circularity (101). However, circularity alone is not convenient enough to accurately establish melanoma thickness, thus a third classification step was needed.

The third step of the analysis relied on to the dermal localization of melanoma cells. These data are in line with our previous findings as shorter wavelengths, like G and R penetrate the dermis only superficially and are absorbed and reflected by tumor chromophores mainly from the surface (113). The IR wavelengths penetrates deeper to the skin and reflected by chromophores of melanomas deeper from the dermis (114) consistently with the literature (115). Therefore, G channel was convenient to differentiate between Breslow≤1 mm melanomas and Breslow:1-2 mm melanomas, whereas the IR channel was capable of to distinguish between Breslow:1-2 mm melanomas and melanomas with higher than 2mm Breslow thickness. Because of its physical characteristics, the G channel was more effective to identify superficial lesions. Thinner melanomas had higher intensities because of the lower melanin concentration, whereas G channel could not differentiate between Breslow:1-2 mm and Breslow>2 mm melanomas. The IR channel was effective to provide information about the deeper layers of the skin. Therefore, it was convenient to distinguish better between Breslow: 1-2 mm and Breslow>2 mm melanomas. Thinner melanomas are characterized by a higher chance for regression and the presence of hypopigmented areas (40). These lesions have higher intensity values in both G and IR channels.

In this study, we also compared the performance of our MSI-based method to human observers. Clinical photographs and dermoscopic images of 100 melanomas were shown

to dermatologists and dermatology residents to determine their dexterity to classify the lesion based on tumor thickness. Dermatologists and dermatology residents completed the form with a total sensitivity of 60.38%, of which the dermatologists reached a sensitivity of 62.19%, and the dermatologist residents operated at a sensitivity rate of 58.44%. Specificity reached 80.86%, with 81.09% and 79.76%, for dermatologists and dermatology residents, respectively. The total agreement was found to be moderate (κ = 0.41; 95% CI, 0.40 to 0.43). Compared to the melanoma classification algorithm, all human investigators achieved a lower sensitivity and specificity in classifying melanomas into subgroups based on presumed histological tumor thickness. Humans had lower accuracy, and the agreement was higher using the algorithm (κ = 0.67; 95% CI, 0.58-0.76). However, it is important to note that palpation is an important guide to clinicians to supplement their vision when they estimate the tumor thickness during routine examinations, which was not possible in this study. This data was similar to earlier findings in the literature. Dermoscopy was recently described to be able to predict Breslow tumor thickness with a concordance of 0.52, and it could even differentiate between in situ melanomas and tumors thicker than 1 mm (63) whereas we did not examine *in situ* melanomas because of their lack of Breslow thickness value.

This MSI technique and our novel algorithm is a potential modality to aid the clinicians in the evaluation of melanoma depth. It is comparable to other tools such as HFUS which could estimate the appropriate surgical margins of melanomas (1, 2 or 3 cm) in 26 of the 31 subjects (41). Furthermore, preoperative HFUS was found to be a potential tool aid for the excision of melanoma in one step (111). Combining HFUS with digital dermoscopy augmented the accuracy and could differentiate thick and thin melanomas with a sensitivity of 86.7% (116). Optical coherence tomography is a potential tool also to predict melanoma tumor thickness based on their vascular morphology (117). Reflectance confocal microscopy proved to be an accurate modality in the presurgical margin mapping of only LMMs (118, 119). Although these imaging modalities can be used to estimate Breslow tumor thickness, compared to MSI, their main disadvantage is that they are expensive, and their efficacy depends fundamentally on the examiner's skill and proficiency (120, 121) (122).

In this paper our second aim was to distinguish melanoma from seborrheic keratosis. The differentiation of SK from melanoma is crucial. Even the most experienced dermatologists miss the diagnosis of skin tumors working with a hit rate of 75-80% and it is worse among general physicians (81). A retrospective study analyzed 9204 cases where the clinical diagnosis was seborrheic keratosis, and 0,7% of them proved to be melanoma after the clinical diagnosis (45). As we have shown in the previous study, the first step of our algorithm differentiating melanoma from other pigmented lesions, like pigmented nevi is not easy and is even more frequent on unusual skin sites, such as the foot (123). Delayed diagnosis of melanoma leads to dramatically lower life expectancy (124) and higher risk of metastatic disease (27).

There is an emerging number of multispectral imaging techniques in the market developed to diagnose skin diseases since 1994 (69, 125). Many of these techniques became commercialized, such as SIAscope (126) and SpectroShade (103) to help the diagnosis of melanoma . Nonetheless, their high price and unsatisfactory specificity limits their use in the everyday clinical practice (76, 127). Compared to these our device is potentially cheaper and easier to apply based on our findings working with a high sensitivity and specificity.

In this study we compared melanoma to SK with a LED-based modality, using multiple quantitative parameters. In the AF images of SKs, based on the comparison to dermoscopy images, high intensity values were mainly caused by the milia-like cysts and comedo-like openings, which are primarily consist of keratin (128). However, keratin is not solely responsible for the high intensity values, NADH, FAD, complex structures, lipid particles may also be responsible for higher AF signal (129, 130). Compared to SKs, melanoma images had lower AF intensity values, in agreement with the data in the literature (131, 132). The presence of melanin, which has a very specific absorption pattern, could be the explanation for the lower AF signal, (131), but the altered collagen structure caused by the tumor growth may also play a part. (133, 134). Melanin acts as a nonfluorescent pigment under UV and short wavelength visible light; it only bear with fluorescent characteristics under near-infrared light (135). The latter has been confirmed with our measurements, where melanin appeared as a dark nonfluorescent pigment visualized with AF, G and R channels without fluorescent emission. Both AF/G and AF/R

ratios were significantly higher in SK, which is caused by mainly the high values in the AF channel. The average AF intensity of the SK lesion was significantly higher also compared to melanomas, which was in line with the Min/Max ratios, where the minimum values were significantly higher in SKs.

The results of the particle analysis were also remarkable, but the standard deviation was high. There were also some hindrances where hyperkeratosis or ulcerations on the surface of the melanomas made the analysis inaccurate. Moreover, overexposed images of SKs are not suitable for this analysis, because their signal level does not fit the auto thresholding and they have resulted in very low values among the SKs despite their high number of highly autofluorescent particles. Accordingly, the right length of exposure is crucial during the image procurement.

Our novel SK index could differentiate melanomas from SKs with a sensitivity of 91.9% and specificity of 57.0%. This method may have a great potential to screen melanomas in the everyday practice among general physicians (GPs), as it is capable of the differentiation of melanomas from benign SKs. Nowadays the computer assisted melanoma diagnosis is focusing on the differential diagnosis of melanoma from pigmented lesions, mostly nevi. There are many promising tools and applications, many of them has very high sensitivities and specificities (76), and they often use artificial intelligence based computer-assisted devices (CAD) to differentiate the lesions According to a meta-analysis of 8 studies, CAD using multispectral images can differentiate melanoma with an average sensitivity of 92.9% and specificity of 43.6% which data is comparable with our findings (136).

Similar studies have been carried out using different imaging techniques, including Raman spectroscopy where it proved to be applicable to differentiate malignant skin lesions from benign lesions, where 147 SKs were in the benign subgroup. This technique had a 99% of sensitivity and a specificity of 33.5% and in the beginning and the developer group achieved a sensitivity of 90% and specificity of 82.1 %. till the end phase of the development. These data is comparable to our findings with high sensitivities and specificities; however, Raman spectroscopy is expensive and not easily accessible tool and can be hardly implemented to the everyday practice to a general physician but would be an excellent modality in specialized skin cancer centers. LED-based MSI is a more

accessible device which would be suitable in a non-expert practice to screen patients to differentiate melanoma form seborrheic keratoses.

Teledermatology and skin imaging are rapidly evolving fields of dermatology, giving patients the opportunity to be both subjects and users of the test method. An increasing number of new applications are appearing with continuously improving performance (93, 137, 138). Our novel approach to MM and its differentiation was a CMOS camera using LED-based multispectral imaging techniques. We found that MM can be distinguished from SK based on differences in intensity and shape characteristics and this method is also applicable to estimate Breslow tumor thickness. However, shape features did not provide as accurate information as intensity parameters due to the properties of nodular melanomas. Particle analysis can be useful and can confirm the diagnosis because it can detect milia-like cysts and comedo-like orifices that give an intense AF signal. The further development and fine-tuning of this method could render multispectral imaging available in the everyday practice to help general physicians to differentiate MMs from SKs. Also, in challenging situations it may help surgeons and dermatologists before melanoma operations to estimate the surgical margins better with a new decision support.

5. Conclusion

It is easy-to-access, relatively cheap and can be used as a mobile-add-on device using the camera of a smartphone. Based on our findings:

1) MSI may be used in clinical practice for the prediction of appropriate safety margins for curative melanoma excisions. MSI is a potential tool to determine the required surgical margin based on the estimated Breslow thickness.

2) Parameter *s'* is a potential first step to differentiate nevi from melanomas to rule them out from the melanoma tumor depth determination

3) We found that melanoma can be differentiated from SK with the use of intensity descriptors and particle analysis.

4) SK index is a potential algorithm to differentiate melanoma from SK, and it is even able to differentiate the melanoma-mimicking MM-like SKs from melanoma and the SK-like MM's from SKs.

5) The collected data may serve as a training pool for machine learning algorithms for further improvements in order to achieve a more accurate estimation of Breslow thickness.

6. Summary

Dermoscopy is a tool designed for healthcare professionals with dedicated training (63, 112, 139) whereas MSI requires no previous training and may be used as smartphones attachment to estimate tumor thickness. The subjectiveness of clinical examinations in dermatology is very high, and there is an emerging need of objective quantitative parameters. This imaging algorithm implemented into this cost-effective tool may help the everyday practice of general physicians in the future. It can help to determine the Breslow tumor thickness of melanoma and it can differentiate melanoma from seborrheic keratosis. We believe that our findings may very well be used for future artificial intelligence analysis.

7. References

1. Surveillance, Epidemiology, and End Results (SEER) Program. SEER*Stat Database: Incidence-SEER 9 Regs Research Data,<Katrina/Rita Population Adjustment>-Linked To County Attributes-Total US, 1969-2017 Counties. National Cancer Institute, Division of Cancer Control and Population Sciences, Surveillance Research Program; 2019., Nov. 2018 Sub (1973-2016)

2. Matthews NH, Li W-Q, Qureshi AA, Weinstock MA, Cho E. (2017) Cutaneous melanoma: etiology and therapy. Chapter 1Epidemiology of Melanoma.

3. Schadendorf D, van Akkooi AC, Berking C, Griewank KG, Gutzmer R, Hauschild A, Stang A, Roesch A, Ugurel S. (2018) Melanoma. The Lancet, 392: 971-984.

4. Rastrelli M, Tropea S, Rossi CR, Alaibac M. (2014) Melanoma: epidemiology, risk factors, pathogenesis, diagnosis and classification. In vivo, 28: 1005-1011.

5. Gandini S, Sera F, Cattaruzza MS, Pasquini P, Picconi O, Boyle P, Melchi CF. (2005) Meta-analysis of risk factors for cutaneous melanoma: II. Sun exposure. European journal of cancer, 41: 45-60.

6. Wu S, Han J, Laden F, Qureshi AA. (2014) Long-term Ultraviolet Flux, Other Potential Risk Factors, and Skin Cancer Risk: A Cohort StudyUltraviolet Flux, Other Risk Factors, and Skin Cancer. Cancer epidemiology, biomarkers & prevention, 23: 1080-1089.

7. Olsen CM, Carroll HJ, Whiteman DC. (2010) Estimating the attributable fraction for melanoma: a meta-analysis of pigmentary characteristics and freckling. International journal of cancer, 127: 2430-2445.

8. Gandini S, Sera F, Cattaruzza MS, Pasquini P, Abeni D, Boyle P, Melchi CF. (2005) Meta-analysis of risk factors for cutaneous melanoma: I. Common and atypical naevi. European journal of cancer, 41: 28-44.

9. Watt AJ, Kotsis SV, Chung KC. (2004) Risk of melanoma arising in large congenital melanocytic nevi: a systematic review. Plastic and reconstructive surgery, 113: 1968-1974.

10. Pampena R, Kyrgidis A, Lallas A, Moscarella E, Argenziano G, Longo C. (2017) A meta-analysis of nevus-associated melanoma: Prevalence and practical implications. Journal of the American Academy of Dermatology, 77: 938-945. e934.

11. Ingraffea A. (2013) Melanoma. Facial Plastic Surgery Clinics, 21: 33-42.

12. Ward WH, Farma JM. (2017) Cutaneous melanoma: etiology and therapy [Internet].

13. Albert DM, Niffenegger AS, Willson JK. (1992) Treatment of metastatic uveal melanoma: review and recommendations. Survey of ophthalmology, 36: 429-438.

14. Yde SS, Sjoegren P, Heje M, Stolle LB. (2018) Mucosal melanoma: a literature review. Current oncology reports, 20: 1-10.

15. Bolognia JL, Jorizzo JL, Schaffer JV. Dermatology e-book. Elsevier Health Sciences2012.

16. Braun RP, Rabinovitz HS, Krischer J, Kreusch J, Oliviero M, Naldi L, Kopf AW, Saurat JH. (2002) Dermoscopy of pigmented seborrheic keratosis: a morphological study. Archives of dermatology, 138: 1556-1560.

17. Elbaum M, Kopf AW, Rabinovitz HS, Langley RG, Kamino H, Mihm Jr MC, Sober AJ, Peck GL, Bogdan A, Gutkowicz-Krusin D. (2001) Automatic differentiation of melanoma from melanocytic nevi with multispectral digital dermoscopy: a feasibility study. Journal of the American Academy of Dermatology, 44: 207-218.

18. Mun JH, Kim GW, Jwa SW, Song M, Kim HS, Ko HC, Kim BS, Kim MB. (2013) Dermoscopy of subungual haemorrhage: its usefulness in differential diagnosis from nail-unit melanoma. British Journal of Dermatology, 168: 1224-1229.

19. Fargnoli MC, Kostaki D, Piccioni A, Micantonio T, Peris K. (2012) Dermoscopy in the diagnosis and management of non-melanoma skin cancers. European Journal of Dermatology, 22: 456-463.

20. Zalaudek I, Ferrara G, Leinweber B, Mercogliano A, D'Ambrosio A, Argenziano G. (2005) Pitfalls in the clinical and dermoscopic diagnosis of pigmented actinic keratosis. Journal of the American Academy of Dermatology, 53: 1071-1074.

21. Braga JCT, Scope A, Klaz I, Mecca P, Spencer P, Marghoob AA. (2008) Melanoma mimicking seborrheic keratosis: an error of perception precluding correct dermoscopic diagnosis. Journal of the American Academy of Dermatology, 58: 875-880.

22. Carrera C, Segura S, Aguilera P, Takigami CM, Gomes A, Barreiro A, Scalvenzi M, Longo C, Cavicchini S, Thomas L. (2017) Dermoscopy improves the diagnostic accuracy of melanomas clinically resembling seborrheic keratosis: cross-sectional study of the ability to detect seborrheic keratosis-like melanomas by a group of dermatologists with varying degrees of experience. Dermatology, 233: 471-479.

23. Swetter SM, Tsao H, Bichakjian CK, Curiel-Lewandrowski C, Elder DE, Gershenwald JE, Guild V, Grant-Kels JM, Halpern AC, Johnson TM. (2019) Guidelines of care for the management of primary cutaneous melanoma. Journal of the American Academy of Dermatology, 80: 208-250.

24. Sober AJ, Chuang T-Y, Duvic M, Farmer ER, Grichnik JM, Halpern AC, Ho V, Holloway V, Hood AF, Johnson TM. (2001) Guidelines of care for primary cutaneous melanoma. Journal of the American Academy of Dermatology, 45: 579-586.

25. Meyer N, Lauwers-Cances V, Lourari S, Laurent J, Konstantinou MP, Lagarde JM, Krief B, Batatia H, Lamant L, Paul C. (2014) High-frequency ultrasonography but not 930-nm optical coherence tomography reliably evaluates melanoma thickness in vivo: a prospective validation study. British Journal of Dermatology, 171: 799-805.

26. Davis LE, Shalin SC, Tackett AJ. (2019) Current state of melanoma diagnosis and treatment. Cancer biology & therapy, 20: 1366-1379.

27. Kandel M, Allayous C, Dalle S, Mortier L, Dalac S, Dutriaux C, Leccia M, Guillot B, Saiag P, Lacour J. (2018) Update of survival and cost of metastatic melanoma with new drugs: Estimations from the MelBase cohort. European Journal of Cancer, 105: 33-40.

28. Sladden MJ, Balch C, Barzilai DA, Berg D, Freiman A, Handiside T, Hollis S, Lens MB, Thompson JF. (2009) Surgical excision margins for primary cutaneous melanoma. Cochrane Database of Systematic Reviews.

29. Gershenwald JE, Scolyer RA, Hess KR, Sondak VK, Long GV, Ross MI, Lazar AJ, Faries MB, Kirkwood JM, McArthur GA. (2017) Melanoma staging: evidence-based changes in the American Joint Committee on Cancer eighth edition cancer staging manual. CA: a cancer journal for clinicians, 67: 472-492.

30. Coit DG, Andtbacka R, Anker CJ, Bichakjian CK, Carson WE, 3rd, Daud A, Dilawari RA, Dimaio D, Guild V, Halpern AC, Hodi FS, Jr., Kelley MC, Khushalani NI, Kudchadkar RR, Lange JR, Lind A, Martini MC, Olszanski AJ, Pruitt SK, Ross MI, Swetter SM, Tanabe KK, Thompson JA, Trisal V, Urist MM. (2012) Melanoma. J Natl Compr Canc Netw, 10: 366-400.

31. Cassileth BR, Lusk EJ, Tenaglia AN. (1983) Patients' perceptions of the cosmetic impact of melanoma resection. Plastic and reconstructive surgery, 71: 73-75.

32. Tamošiūnas M, Plorina EV, Lange M, Derjabo A, Kuzmina I, Bļizņuks D, Spigulis J. (2020) Autofluorescence imaging for recurrence detection in skin cancer postoperative scars. Journal of Biophotonics, 13: e201900162.

33. Koshenkov VP, Broucek J, Kaufman HL. (2016) Surgical management of melanoma. Melanoma: 149-179.

34. Koshenkov VP, Shulkin D, Bustami R, Chevinsky AH, Whitman ED. (2012) Role of sentinel lymphadenectomy in thin cutaneous melanomas with positive deep margins on initial biopsy. Journal of surgical oncology, 106: 363-368.

35. Edge SB, Byrd DR, Carducci MA, Compton CC, Fritz A, Greene F. AJCC cancer staging manual Vol. 7. Springer New York2010.

36. Michielin O, van Akkooi A, Lorigan P, Ascierto P, Dummer R, Robert C, Arance A, Blank C, Sileni VC, Donia M. (2020) ESMO consensus conference recommendations on the management of locoregional melanoma: under the

auspices of the ESMO Guidelines Committee. Annals of Oncology, 31: 1449-1461.

37. Keilholz U, Ascierto P, Dummer R, Robert C, Lorigan P, van Akkooi A, Arance A, Blank C, Sileni VC, Donia M. (2020) ESMO consensus conference recommendations on the management of metastatic melanoma: under the auspices of the ESMO Guidelines Committee. Annals of Oncology, 31: 1435-1448.

38. Kittler H, Pehamberger H, Wolff K, Binder M. (2002) Diagnostic accuracy of dermoscopy. The lancet oncology, 3: 159-165.

39. Pehamberger H, Steiner A, Wolff K. (1987) In vivo epiluminescence microscopy of pigmented skin lesions. I. Pattern analysis of pigmented skin lesions. Journal of the American Academy of Dermatology, 17: 571-583.

40. Rodríguez-Lomba E, Lozano-Masdemont B, Nieto-Benito LM, Hernández de la Torre E, Suárez-Fernández R, Avilés-Izquierdo JA. (2021) Dermoscopic Predictors of Tumor Thickness in Cutaneous Melanoma: A Retrospective Analysis of 245 Melanomas. Dermatol Pract Concept, 11: e2021059.

41. Machet L, Belot V, Naouri M, Boka M, Mourtada Y, Giraudeau B, Laure B, Perrinaud A, Machet M-C, Vaillant L. (2009) Preoperative measurement of thickness of cutaneous melanoma using high-resolution 20 MHz ultrasound imaging: A monocenter prospective study and systematic review of the literature. Ultrasound in medicine & biology, 35: 1411-1420.

42. Hartmann D, Krammer S, Ruini C, Ruzicka T, von Braunmühl T. (2016) Correlation of histological and ex-vivo confocal tumor thickness in malignant melanoma. Lasers in medical science, 31: 921-927.

43. Oh J-T, Li M-L, Zhang HF, Maslov K, Wang LV. (2006) Three-dimensional imaging of skin melanoma in vivo by dual-wavelength photoacoustic microscopy. Journal of biomedical optics, 11: 034032.

44. Wollina U. (2019) Recent advances in managing and understanding seborrheic keratosis. F1000Research, 8.

45. Izikson L, Sober AJ, Mihm MC, Zembowicz A. (2002) Prevalence of melanoma clinically resembling seborrheic keratosis: analysis of 9204 cases. Archives of dermatology, 138: 1562-1566.

46. Rubegni P, Feci L, Nami N, Burroni M, Taddeucci P, Miracco C, Munezero Butorano MA, Fimiani M, Cevenini G. (2015) Computer-assisted melanoma diagnosis: a new integrated system. Melanoma research, 25: 537-542.

47. Marghoob A, Braun R. An atlas of dermoscopy. CRC Press2012.

48. Weedon D. Weedon's Skin Pathology E-Book: Expert Consult-Online and Print. Elsevier Health Sciences2009.

49. Clebak K. (2020) Dermatoscopy and Skin Cancer: A Handbook for Hunters of Skin Cancer and Melanoma. Family Medicine, 52: 148-149.

50. Takenouchi T. (2011) Key points in dermoscopic diagnosis of basal cell carcinoma and seborrheic keratosis in Japanese. The Journal of dermatology, 38: 59-65.

51. Minagawa A. (2017) Dermoscopy–pathology relationship in seborrheic keratosis. The Journal of Dermatology, 44: 518-524.

52. Greco MJ, Bhutta BS. Seborrheic keratosis. In: StatPearls [Internet]. StatPearls Publishing, 2021.

53. Carrera C, Segura S, Aguilera P, Scalvenzi M, Longo C, Barreiro A, Broganelli P, Cavicchini S, Llambrich A, Zaballos P. (2017) Dermoscopic clues for diagnosing melanomas that resemble seborrheic keratosis. JAMA dermatology, 153: 544-551.

54. Carrera C, Marchetti MA, Dusza SW, Argenziano G, Braun RP, Halpern AC, Jaimes N, Kittler HJ, Malvehy J, Menzies SW, Pellacani G, Puig S, Rabinovitz HS, Scope A, Soyer HP, Stolz W, Hofmann-Wellenhof R, Zalaudek I, Marghoob AA. (2016) Validity and Reliability of Dermoscopic Criteria Used to Differentiate Nevi From Melanoma: A Web-Based International Dermoscopy Society Study. JAMA Dermatol, 152: 798-806.

55. Que SKT. (2016) Research techniques made simple: noninvasive imaging technologies for the delineation of basal cell carcinomas. Journal of Investigative Dermatology, 136: e33-e38.

56. Katz B, Rabinovitz HS. (2001) Introduction to dermoscopy. Dermatologic clinics, 19: 221-258.

57. Lee JB, Hirokawa D. (2010) Dermatoscopy: Facts and controversies. Clinics in dermatology, 28: 303-310.

58. Lake A, Jones B. (2015) Dermoscopy: to cross-polarize, or not to cross-polarize, that is the question: A literature review. Journal of visual communication in medicine, 38: 36-50.

59. Benvenuto-Andrade C, Dusza SW, Agero ALC, Scope A, Rajadhyaksha M, Halpern AC, Marghoob AA. (2007) Differences between polarized light dermoscopy and immersion contact dermoscopy for the evaluation of skin lesions. Archives of dermatology, 143: 329-338.

60. Lacarrubba F, Verzì AE, Micali G. (2015) Newly described features resulting from high-magnification dermoscopy of tinea capitis. Jama Dermatology, 151: 308-310.

61. Marghoob AA, Usatine R, Jaimes N. (2013) Dermoscopy for the family physician. American family physician, 88: 441-450.

62. Chappuis P, Duru G, Marchal O, Girier P, Dalle S, Thomas L. (2016) Dermoscopy, a useful tool for general practitioners in melanoma screening: a nationwide survey. British Journal of Dermatology, 175: 744-750.

63. Polesie S, Jergéus E, Gillstedt M, Ceder H, Dahlén Gyllencreutz J, Fougelberg J, Johansson Backman E, Pakka J, Zaar O, Paoli J. Can Dermoscopy Be Used to Predict if a Melanoma Is In Situ or Invasive? In: Dermatology practical & conceptual Vol. 11, 2021: e2021079.

64. Gülseren D, Hofmann-Wellenhof R. (2019) Evaluation of dermoscopic criteria for seborrheic keratosis on non-polarized versus polarized dermoscopy. Skin Research and Technology, 25: 801-804.

65. Kuzmina I, Diebele I, Spigulis J, Valeine L, Berzina A, Abelite A. (2011) Contact and contactless diffuse reflectance spectroscopy: potential for recovery monitoring of vascular lesions after intense pulsed light treatment. Journal of Biomedical Optics, 16: 040505.

66. Kuzmina I, Diebele I, Asare L, Kempele A, Abelite A, Jakovels D, Spigulis J. Multispectral imaging of pigmented and vascular cutaneous malformations: the influence of laser treatment. In: Laser Applications in Life Sciences Vol. 7376. International Society for Optics and Photonics, 2010: 73760J.

67. Kuzmina I, Diebele I, Jakovels D, Spigulis J, Valeine L, Kapostinsh J, Berzina A. (2011) Towards noncontact skin melanoma selection by multispectral imaging analysis. Journal of Biomedical optics, 16: 060502.

68. Jolivot R, Benezeth Y, Marzani F. (2013) Skin parameter map retrieval from a dedicated multispectral imaging system applied to dermatology/cosmetology. International journal of biomedical imaging, 2013.

69. Setiadi IC, Nasution AM, Chandra TG. A new LED-based multispectral imaging system for blood and melanin content estimation: The validation. In: AIP Conference Proceedings Vol. 2193. AIP Publishing LLC, 2019: 050017.

70. Cook SE, Palmer MD LC, Shuler M, Franklin D. (2015) Smartphone Mobile Application to Enhance Diagnosis of Skin Cancer: A Guide for the Rural Practitioner.

71. Kuzmina I, Lacis M, Spigulis J, Berzina A, Valeine L. (2015) Study of smartphone suitability for mapping of skin chromophores. Journal of biomedical optics, 20: 090503.

72. Lange M, Bozsányi S, Plorina EV, Lihachev A, Derjabo A. Spectral imaging as a tool for the evaluation of skin cancer post-operative scars. In: Biophotonics—Riga 2020 Vol. 11585. International Society for Optics and Photonics, 2020: 1158506.

73. Lihachev A, Lihacova I, Plorina EV, Lange M, Derjabo A, Spigulis J. (2018) Differentiation of seborrheic keratosis from basal cell carcinoma, nevi and

melanoma by RGB autofluorescence imaging. Biomedical optics express, 9: 1852-1858.

74. Farkas K, Bozsányi S, Plázár D, Bánvölgyi A, Fésűs L, Anker P, Zakariás S, Lihacova I, Lihachev A, Lange M. (2021) Autofluorescence imaging of the skin is an objective non-invasive technique for diagnosing pseudoxanthoma elasticum. Diagnostics, 11: 260.

75. Anker P, Fésűs L, Kiss N, Noll J, Becker K, Kuroli E, Mayer B, Bozsányi S, Lőrincz K, Lihacova I. (2021) Visualization of Keratin with Diffuse Reflectance and Autofluorescence Imaging and Nonlinear Optical Microscopy in a Rare Keratinopathic Ichthyosis. Sensors, 21: 1105.

76. March J, Hand M, Truong A, Grossman D. (2015) Practical application of new technologies for melanoma diagnosis: Part II. Molecular approaches. Journal of the American Academy of Dermatology, 72: 943-958.

77. Haniffa MA, Lloyd JJ, Lawrence CM. (2007) The use of a spectrophotometric intracutaneous analysis device in the real-time diagnosis of melanoma in the setting of a melanoma screening clinic. Br J Dermatol, 156: 1350-1352.

78. Walter FM, Morris HC, Humphrys E, Hall PN, Prevost AT, Burrows N, Bradshaw L, Wilson EC, Norris P, Walls J. (2012) Effect of adding a diagnostic aid to best practice to manage suspicious pigmented lesions in primary care: randomised controlled trial. Bmj, 345.

79. MacLellan AN, Price EL, Publicover-Brouwer P, Matheson K, Ly TY, Pasternak S, Walsh NM, Gallant CJ, Oakley A, Hull PR. (2021) The use of noninvasive imaging techniques in the diagnosis of melanoma: a prospective diagnostic accuracy study. Journal of the American Academy of Dermatology, 85: 353-359.

80. Huang D, Swanson EA, Lin CP, Schuman JS, Stinson WG, Chang W, Hee MR, Flotte T, Gregory K, Puliafito CA. (1991) Optical coherence tomography. science, 254: 1178-1181.

81. Calzavara-Pinton P, Longo C, Venturini M, Sala R, Pellacani G. (2008) Reflectance confocal microscopy for in vivo skin imaging. Photochemistry and photobiology, 84: 1421-1430.

82. Pellacani G, Guitera P, Longo C, Avramidis M, Seidenari S, Menzies S. (2007) The impact of in vivo reflectance confocal microscopy for the diagnostic accuracy of melanoma and equivocal melanocytic lesions. Journal of investigative dermatology, 127: 2759-2765.

83. Raffin D, Zaragoza J, Georgescou G, Mourtada Y, Maruani A, Ossant F, Patat F, Vaillant L, Machet L. (2017) High-frequency ultrasound imaging for cutaneous neurofibroma in patients with neurofibromatosis type I. European Journal of Dermatology, 27: 260-265.

84. DeJong HM, Abbott S, Zelesco M, Kennedy BF, Ziman MR, Wood FM. (2017) The validity and reliability of using ultrasound elastography to measure cutaneous stiffness, a systematic review. International journal of burns and trauma, 7: 124.

85. Hernandez-Ibanez C, Blazquez-Sanchez N, Aguilar-Bernier M, Fúnez-Liébana R, Rivas-Ruiz F, de Troya-Martin M. (2017) Usefulness of high-frequency ultrasound in the classification of histologic subtypes of primary basal cell carcinoma. Actas Dermo-Sifiliográficas (English Edition), 108: 42-51.

86. Martorell A, Wortsman X, Alfageme F, Roustan G, Arias-Santiago S, Catalano O, Di Santolo MS, Zarchi K, Bouer M, Gaitini D. (2017) Ultrasound evaluation as a complementary test in hidradenitis suppurativa: proposal of a standarized report. Dermatologic Surgery, 43: 1065-1073.

87. Reginelli A, Belfiore MP, Russo A, Turriziani F, Moscarella E, Troiani T, Brancaccio G, Ronchi A, Giunta E, Sica A. (2020) A preliminary study for quantitative assessment with HFUS (High-Frequency Ultrasound) of nodular skin melanoma breslow thickness in adults before surgery: Interdisciplinary team experience. Current radiopharmaceuticals, 13: 48-55.

88. Gambichler T, Jaedicke V, Terras S. (2011) Optical coherence tomography in dermatology: technical and clinical aspects. Archives of dermatological research, 303: 457-473.

89. Olsen J, Holmes J, Jemec GB. (2018) Advances in optical coherence tomography in dermatology—a review. Journal of biomedical optics, 23: 040901.

90. Ferris LK, Harris RJ. (2012) New diagnostic aids for melanoma. Dermatologic clinics, 30: 535-545.

91. Pellacani G, Pepe P, Casari A, Longo C. (2014) Reflectance confocal microscopy as a second-level examination in skin oncology improves diagnostic accuracy and saves unnecessary excisions: a longitudinal prospective study. British Journal of Dermatology, 171: 1044-1051.

92. Lihachev A, Derjabo A, Ferulova I, Lange M, Lihacova I, Spigulis J. (2015) Autofluorescence imaging of basal cell carcinoma by smartphone RGB camera. Journal of Biomedical Optics, 20: 120502.

93. Clark AK, Bosanac S, Ho B, Sivamani RK. (2018) Systematic review of mobile phone-based teledermatology. Archives of Dermatological Research, 310: 675-689.

94. Jobbágy A, Meznerics F, Farkas K, Bozsányi S, Fesus L, Kiss N, Lorincz K, Wikonkal N, Sárdy M, Bánvölgyi A. (2021) 065 Application of teledermatology during the first wave of the COVID-19 pandemic in Hungary. The Journal of Investigative Dermatology, 141: S159.

95. Spigulis J. (2017) Multispectral, fluorescent and photoplethysmographic imaging for remote skin assessment. Sensors, 17: 1165.

96. Diebele I, Bekina A, Derjabo A, Kapostinsh J, Kuzmina I, Spigulis J. Analysis of skin basalioma and melanoma by multispectral imaging. In: Biophotonics: Photonic Solutions for Better Health Care III Vol. 8427. International Society for Optics and Photonics, 2012: 842732.

97. Lihacova I, Bolochko K, Plorina EV, Lange M, Lihachev A, Bliznuks D, Derjabo A. A method for skin malformation classification by combining multispectral and skin autofluorescence imaging. In: Biophotonics: Photonic solutions for better health care VI Vol. 10685. International Society for Optics and Photonics, 2018: 1068535.

98. Lihacova I, Bolocko K, Lihachev A. Semi-automated non-invasive diagnostics method for melanoma differentiation from nevi and pigmented basal cell carcinomas. In: Biophotonics—Riga 2017 Vol. 10592. International Society for Optics and Photonics, 2017: 1059206.

99. Lange M, Kiss N, Fesus L, Plorina EV, Derjabo A, Spigulis J. Non-invasive LED-based screening solution for skin cancer. In: European Conference on Biomedical Optics. Optical Society of America, 2019: 11073_11017.

100. Abràmoff MD, Magalhães PJ, Ram SJ. (2004) Image processing with ImageJ. Biophotonics international, 11: 36-42.

101. Kern AJ, Schlomer BJ, Timberlake MD, Peters CA, Hammer MR, Jacobs MA. (2017) Simple visual review of pre-to post-operative renal ultrasound images predicts pyeloplasty success equally as well as geometric measurements: a blinded comparison with a gold standard. Journal of Pediatric Urology, 13: 401. e401-401. e407.

102. Janssen AF, Breusegem SY, Larrieu D. (2022) Current methods and pipelines for image-based quantitation of nuclear shape and nuclear envelope abnormalities. Cells, 11: 347.

103. Tomatis S, Carrara M, Bono A, Bartoli C, Lualdi M, Tragni G, Colombo A, Marchesini R. (2005) Automated melanoma detection with a novel multispectral imaging system: results of a prospective study. Physics in medicine & biology, 50: 1675.

104. Carrara M, Bono A, Bartoli C, Colombo A, Lualdi M, Moglia D, Santoro N, Tolomio E, Tomatis S, Tragni G. (2007) Multispectral imaging and artificial neural network: mimicking the management decision of the clinician facing pigmented skin lesions. Physics in Medicine & Biology, 52: 2599.

105. Diebele I, Kuzmina I, Kapostinsh J, Derjabo A, Spigulis J. Melanoma-nevus differentiation by multispectral imaging. In: European Conference on Biomedical Optics. Optical Society of America, 2011: 80872G.

106. Marchesini R, Bono A, Tomatis S, Bartoli C, Colombo A, Lualdi M, Carrara M. (2007) In vivo evaluation of melanoma thickness by multispectral imaging and an

artificial neural network. A retrospective study on 250 cases of cutaneous melanoma. Tumori Journal, 93: 170-177.

107. Esteva A, Kuprel B, Novoa RA, Ko J, Swetter SM, Blau HM, Thrun S. (2017) Dermatologist-level classification of skin cancer with deep neural networks. Nature, 542: 115-118.

108. Rastgoo M, Garcia R, Morel O, Marzani F. (2015) Automatic differentiation of melanoma from dysplastic nevi. Computerized Medical Imaging and Graphics, 43: 44-52.

109. Wells A, Patel S, Lee JB, Motaparthi K. (2021) Artificial intelligence in dermatopathology: Diagnosis, education, and research. Journal of Cutaneous Pathology, 48: 1061-1068.

110. Maron RC, Haggenmüller S, von Kalle C, Utikal JS, Meier F, Gellrich FF, Hauschild A, French LE, Schlaak M, Ghoreschi K. (2021) Robustness of convolutional neural networks in recognition of pigmented skin lesions. European journal of cancer, 145: 81-91.

111. Chaput L, Laurent E, Pare A, Sallot A, Mourtada Y, Ossant F, Vaillant L, Patat F, Machet L. (2018) One-step surgical removal of cutaneous melanoma with surgical margins based on preoperative ultrasound measurement of the thickness of the melanoma. European Journal of Dermatology, 28: 202-208.

112. Martínez-Piva M, Vacas A, Kowalczuk MR, Gallo F, Vasconcelos MR, Mazzuoccolo L. (2021) Dermoscopy as a Tool for Estimating Breslow Thickness in Melanoma. Actas Dermo-Sifiliográficas (English Edition), 112: 434-440.

113. Bozsányi S, Farkas K, Bánvölgyi A, Lőrincz K, Fésűs L, Anker P, Zakariás S, Jobbágy A, Lihacova I, Lihachev A. (2021) Quantitative Multispectral Imaging Differentiates Melanoma from Seborrheic Keratosis. Diagnostics, 11: 1315.

114. Lange M, Plorina EV, Lihacova I, Derjabo A, Spigulis J. Skin cancer screening–better safe than sorry. In: SHS Web of Conferences Vol. 85. EDP Sciences, 2020.

115. Ly E, Cardot-Leccia N, Ortonne JP, Benchetrit M, Michiels JF, Manfait M, Piot O. (2010) Histopathological characterization of primary cutaneous melanoma using infrared microimaging: a proof-of-concept study. British Journal of Dermatology, 162: 1316-1323.

116. Pellacani G, Seidenari S. (2003) Preoperative melanoma thickness determination by 20-MHz sonography and digital videomicroscopy in combination. Arch Dermatol, 139: 293-298.

117. De Carvalho N, Welzel J, Schuh S, Themstrup L, Ulrich M, Jemec GB, Holmes J, Kaleci S, Chester J, Bigi L. (2018) The vascular morphology of melanoma is related to Breslow index: an in vivo study with dynamic optical coherence tomography. Experimental dermatology, 27: 1280-1286.

118. Chen CS, Elias M, Busam K, Rajadhyaksha M, Marghoob A. (2005) Multimodal in vivo optical imaging, including confocal microscopy, facilitates presurgical margin mapping for clinically complex lentigo maligna melanoma. British Journal of Dermatology, 153: 1031-1036.

119. Yélamos O, Cordova M, Blank N, Kose K, Dusza SW, Lee E, Rajadhyaksha M, Nehal KS, Rossi AM. (2017) Correlation of handheld reflectance confocal microscopy with radial video mosaicing for margin mapping of lentigo maligna and lentigo maligna melanoma. JAMA dermatology, 153: 1278-1284.

120. Wolner ZJ, Yélamos O, Liopyris K, Rogers T, Marchetti MA, Marghoob AA. (2017) Enhancing skin cancer diagnosis with dermoscopy. Dermatologic clinics, 35: 417-437.

121. Levine A, Markowitz O. (2018) Introduction to reflectance confocal microscopy and its use in clinical practice. JAAD case reports, 4: 1014-1023.

122. Schneider SL, Kohli I, Hamzavi IH, Council ML, Rossi AM, Ozog DM. (2019) Emerging imaging technologies in dermatology: Part II: Applications and limitations. Journal of the American Academy of Dermatology, 80: 1121-1131.

123. Sondermann W, Zimmer L, Schadendorf D, Roesch A, Klode J, Dissemond J. (2016) Initial misdiagnosis of melanoma located on the foot is associated with poorer prognosis. Medicine, 95.

124. Petrie T, Samatham R, Witkowski AM, Esteva A, Leachman SA. (2019) Melanoma Early Detection: Big Data, Bigger Picture. J Invest Dermatol, 139: 25-30.

125. Marchesini R, Ballerini M, Bartoli C, Pignoli E, Sichirollo AE, Tomatis S, Zurrida S, Cascinelli N. Telespectrophotometry of human skin diseases by means of a ccd camera. In: Optical Biopsy Vol. 2081. International Society for Optics and Photonics, 1994: 168-173.

126. Moncrieff M, Cotton S, Hall P, Schiffner R, Lepski U, Claridge E. (2001) SIAscopy assists in the diagnosis of melanoma by utilizing computer vision techniques to visualise the internal structure of the skin. Med Image Underst Anal: 53-56.

127. Ganga RS, Gundre D, Bansal S, Shirsat PM, Prasad P, Desai RS. (2017) Evaluation of the diagnostic efficacy and spectrum of autofluorescence of benign, dysplastic and malignant lesions of the oral cavity using VELscope. Oral oncology, 75: 67-74.

128. Bliznakova I, Borisova E, Avramov L. (2007) Laser-and light-induced autofluorescence spectroscopy of human skin in dependence on excitation wavelengths. ACTA PHYSICA POLONICA SERIES A, 112: 1131.

129. Pal R, Edward K, Ma L, Qiu S, Vargas G. (2017) Spectroscopic characterization of oral epithelial dysplasia and squamous cell carcinoma using multiphoton

autofluorescence micro-spectroscopy. Lasers in surgery and medicine, 49: 866-873.

130. Takahama Jr A, Kurachi C, Cosci A, Faustino ISP, Camisasca DR, Fontes KBdCF, Pires FR, Azevedo RS. (2013) Usefulness of tissue autofluorescence imaging in actinic cheilitis diagnosis. Journal of biomedical optics, 18: 076023.

131. Borisova EG, Angelova LP, Pavlova EP. (2013) Endogenous and exogenous fluorescence skin cancer diagnostics for clinical applications. IEEE Journal of Selected Topics in Quantum Electronics, 20: 211-222.

132. Zonios G, Dimou A, Bassukas I, Galaris D, Tsolakidis A, Kaxiras E. (2008) Melanin absorption spectroscopy: new method for noninvasive skin investigation and melanoma detection. Journal of biomedical optics, 13: 014017.

133. Pratavieira S, Andrade C, Salvio A, Bagnato V, Kurachi C. (2011) Optical imaging as auxiliary tool in skin cancer diagnosis. Skin Cancers–Risk Factors, Prevention and Therapy: 159-173.

134. Fang M, Yuan J, Peng C, Li Y. (2014) Collagen as a double-edged sword in tumor progression. Tumor Biology, 35: 2871-2882.

135. Huang Z, Zeng H, Hamzavi I, Alajlan A, Tan E, McLean DI, Lui H. (2006) Cutaneous melanin exhibiting fluorescence emission under near-infrared light excitation. Journal of biomedical optics, 11: 034010.

136. di Ruffano LF, Takwoingi Y, Dinnes J, Chuchu N, Bayliss SE, Davenport C, Matin RN, Godfrey K, O'Sullivan C, Gulati A. (2018) Computer-assisted diagnosis techniques (dermoscopy and spectroscopy-based) for diagnosing skin cancer in adults. Cochrane Database of Systematic Reviews.

137. Abbott LM, Magnusson RS, Gibbs E, Smith SD. (2018) Smartphone use in dermatology for clinical photography and consultation: Current practice and the law. Australasian Journal of Dermatology, 59: 101-107.

138. Accetta JL, Schoenfeld J, Bitar C, Murina A. (2020) Smartphones in dermatology: acceptance of smartphone photography by the informed patient. Dermatologic Surgery, 46: 1131-1133.

139. Lallas A, Longo C, Manfredini M, Benati E, Babino G, Chinazzo C, Apalla Z, Papageorgiou C, Moscarella E, Kyrgidis A. (2018) Accuracy of dermoscopic criteria for the diagnosis of melanoma in situ. JAMA dermatology, 154: 414-419.

8. Bibliography of the candidate's publications

8.1. Publications directly related to this thesis

Bozsányi, S., Farkas, K., Bánvölgyi, A., Lőrincz, K., Fésűs, L., Anker, P., ... & Wikonkál, N. M. (2021). Quantitative Multispectral Imaging Differentiates Melanoma from Seborrheic Keratosis. *Diagnostics, 11*(8), 1315.

Bozsányi, S., Varga, N. N., Farkas, K., Bánvölgyi, A., Lőrincz, K., Lihacova, I., ... & Wikonkál, N. M. (2022). Multispectral Imaging Algorithm Predicts Breslow Thickness of Melanoma. *Journal of Clinical Medicine, 11*(1), 189.

8.2. Publications indirectly related to this thesis

Anker, P., Fésűs, L., Kiss, N., Noll, J., Becker, K., Kuroli, E., ... & Medvecz, M. (2021). Visualization of Keratin with Diffuse Reflectance and Autofluorescence Imaging and Nonlinear Optical Microscopy in a Rare Keratinopathic Ichthyosis. *Sensors, 21*(4), 1105.

Farkas, K., Bozsányi, S., Plázár, D., Bánvölgyi, A., Fésűs, L., Anker, P., ... & Kiss, N. (2021). Autofluorescence Imaging of the Skin Is an Objective Non-Invasive Technique for Diagnosing Pseudoxanthoma Elasticum. *Diagnostics, 11*(2), 260.

9. Acknowledgement

This project would not have been possible without the support of many people. First of all many thanks to my adviser, my PI, Professor Norbert Wikonkál, who read my numerous revisions and helped make some sense of the confusion. He is like a father for us who helps me also with my career, my academic path and to make better decisions and have clearer aspects in life. Without him I would not be here now.

Thanks to my senior labor members, Dr. András Bánvölgyi and Dr. Kende Lőrincz, who offered guidance and support and helped me with their senior advices during this research. They believed me from the very beginning and in my scientific success when no one believed and encouraged me to do not give up and push forward. Thank you very much!

Thanks to my PhD and resident doctor colleagues, Dr. Klára Farkas, Dr. Antal Jobbágy, Dr. Luca Fésűs, Dr. Pálma Anker, Dr. Sára Pálla, and to our student researchers, Jázmin Shamsodini, Noémi Nóra Varga, Natália Czurkó, Lili Gulyás, István Szondy, and Maxime Buitendijk who helped me countless times during our measurements and without them these results would not be here. Thank you very much!

Thanks to the Semmelweis University, and to the Department of Dermatology, Venereology and Dermatooncology for supporting and helping my research, special thanks to our chair, Prof. Péter Holló for his great support and advices.

I thank also thank Dr. Judit Hársing, Dr. Veronika Tóth, Dr. József Szakonyi, Dr. Daniella Kuzmanovszki, Dr. Béla Tóth, Dr. Hunor Gergely, Dr. Kincső Blága, Dr. Dalma Márton, Dr. Melinda Fábián, Dr. Andor Hodossy- Virágh, Dr. Tünde Kerner, Dr. Martina Kádas, Dr. Dóra Faluhelyi, Dr. Cecília Nagy, Dr. Sarolta Sándor and Dr. Dénes Póta who took part in the clinical care of the patients. We thank Dr. Eleonóra Imrédi, Dr. Mariann Müller, Dr. Veronika Tóth, Dr. Cecília Nagy, Dr. Ugur Cakir, Dr. Daniella Kuzmanovszki, Dr. Pálma Anker, Dr. Kincső Blága, Dr. Zsófia Tari, Dr. KarolinaPolgár, Dr. József Szakonyi , Isolde Joura, Dr. Laura Belvon and Dr. Eszter Müller for helping in the spreadsheet questionnaire.

We thank Ilze Lihacova, Alexey Lihachev, Emilija Vija Plorina, Marta Lange, Dmitrijs Bļizņuks, Emilija Vija Plorina and the University of Latvia for the development and for being the best collaborator partners during these studies, we could always count on you.

And last but not least, I would like to thank Dr. Norbert Kiss, my mentor, who helped me through this PhD journey. I have received and learnt countless things from him, who was always understanding, helpful and kind to me. He is like a big brother for me and I hope I can give back all the good things to him I have received during these PhD years. Thank you!

Funding: This work was supported by grants from the EFOP-3.6.3-VEKOP-16-2017-00009 (S.B., N.N.V.) EFOP-3.6.3-VEKOP-16 (S.B.) the ÚNKP-21-4-II-SE-10 (N.K.) and ÚNKP-20-3-I-SE-24 (S.Z.) New National Excellence Program of the Ministry For Innovation and Technology from the source of the National Research, Development and Innovation Fund of Hungary and the European Regional Development Fund projects "Time-resolved autofluorescence methodology for noninvasive skin cancer diagnostics" [No. 1.1.1.2/16/I/001, agreement No. 1.1.1.2/VIAA/1/16/014 (A.L.)] and "Development and clinical validation of a novel cost effective multi-modal method-ology for early diagnostics of skin cancers" [No. 1.1.1.2/16/I/001 agreement No. 1.1.1.2/VIAA/1/16/052 (I.L.)], the National Research, Development and Innovation Office of Hungary—NKFIH (FK_131916, 2019 [Semmelweis University, M.M.)], European Regional Development Fund project "Development and clinical validation of a novel cost effective multi-modal methodology for early diagnostics of skin cancers" [No. 1.1.1.2/16/I/001 agreement No. 1.1.1.2/VIAA/1/16/052 (I.L.)] and the Latvian Council of Science project "Skin cancer early diagnostics accuracy improvement by using neural networks," [No. lzp-2018/2-0052 (I.L., A.L).